1   **Ubiquitin ligases and a processive proteasome facilitate protein clearance**

2   **during the oocyte-to-embryo transition in *Caenorhabditis elegans***

3

4   **Caroline A. Spike*, Tatsuya Tsukamoto*, and David Greenstein*,[1]**

5

6   *Department of Genetics, Cell Biology and Development, University of Minnesota,

7   Minneapolis, Minnesota 55455, USA

8

9   Running title: Protein Degradation During the OET

10

11   Keywords: oocyte meiotic maturation, oocyte-to-embryo transition, translational regulation,

12   RNA-binding proteins, ubiquitin-mediated protein degradation

13

14   [1]Corresponding author: David Greenstein, Department of Genetics, Cell Biology, and

15   Development, University of Minnesota, 4-208 MCB, 420 Washington Avenue SE, Minneapolis,

16   MN 55455. Tel: 612-624-3955; FAX: 612-626-6140. E-mail: green959@umn.edu

17

ABSTRACT

The ubiquitin-mediated degradation of oocyte translational regulatory proteins is a conserved feature of the oocyte-to-embryo transition (OET). In the nematode *Caenorhabditis elegans*, multiple translational regulatory proteins, including the TRIM-NHL RNA-binding protein LIN-41/Trim71 and the Pumilio-family RNA-binding proteins PUF-3 and PUF-11, are degraded during the OET. Degradation of each protein requires activation of the M-phase cyclin-dependent kinase CDK-1, is largely complete by the end of the first meiotic division and does not require the anaphase promoting complex (APC). However, only LIN-41 degradation requires the F-box protein SEL-10/FBW7/Cdc4p, the substrate recognition subunit of an SCF-type E3 ubiquitin ligase. This finding suggests that PUF-3 and PUF-11, which localize to LIN-41-containing ribonucleoprotein particles (RNPs), are independently degraded through the action of other factors and that the oocyte RNPs are disassembled in a concerted fashion during the OET. We develop and test the hypothesis that PUF-3 and PUF-11 are targeted for degradation by the proteasome-associated HECT-type ubiquitin ligase ETC-1/UBE3C/Hul5, which is broadly expressed in *C. elegans*. We find that several GFP-tagged fusion proteins that are degraded during the OET, including fusions with PUF-3, PUF-11, LIN-41, IFY-1/Securin and CYB-1/Cyclin B, are incompletely degraded when ETC-1 function is compromised. However, it is the fused GFP moiety that appears to be the critical determinant of this proteolysis defect. These findings are consistent with a conserved role for ETC-1 in promoting proteasome processivity and suggest that proteasomal processivity is an important element of the OET during which many key oocyte regulatory proteins are rapidly targeted for degradation.

39

3

Article Summary

The ubiquitin-mediated degradation of translational regulatory RNA-binding proteins is a conserved feature of the oocyte-to-embryo transition (OET). *C. elegans* LIN-41 is a master regulator of oogenesis and is found in a large translational regulatory ribonucleoprotein (RNP) complex with more than 1000 maternal transcripts and the Pumilio-family RNA-binding proteins PUF-3 and PUF-11. We show that the concerted action of ubiquitin-mediated protein degradation and proteasome processivity rapidly disassemble LIN-41-containing RNPs during the OET thereby relieving repression of many maternal transcripts.

INTRODUCTION

The oocyte-to-embryo transition (OET) initiates when oocytes exit meiotic prophase and enter the first meiotic metaphase, a cell cycle and developmental event also known as meiotic resumption or meiotic maturation. The OET is complete when zygotic gene transcription begins after fertilization in the early embryo. In many mammals and in the nematode *Caenorhabditis elegans*, zygotic gene transcription begins early at the 2- or ~4-cell stage, respectively (Clegg and Pikó 1982; Latham *et al*. 1991; Edgar *et al*., 1994; Seydoux and Fire 1994; Hamatani *et al*. 2004). In some animals, such as Drosophila and Xenopus, zygotic gene activation predominantly begins later—at approximately the eighth nuclear division in Drosophila (Pritchard and Schubiger 1996; reviewed by Harrison and Eisen 2015) and at the midblastula transition in Xenopus (Bachvarova *et al.* 1966; Newport and Kirschner 1982a,b; reviewed by Blitz and Cho 2021). Because the late-stage oocytes of most animals are transcriptionally quiescent, the regulation of protein translation by RNA-binding proteins represents a dominant mode of developmental control during oocyte meiotic maturation and the OET (reviewed by Kotani *et al*. 2017; Huelgas-Morales and Greenstein 2018; Teixeira and Lehmann 2019). In fact, genomic analyses suggest that mammalian oocytes contain more than 200 RNA-binding proteins (Luong and Conti 2019). The presumption is that many of these RNA-binding proteins regulate protein translation in oocytes and preserve the dowry of maternal mRNA contributed to the early embryo.

In *C. elegans* oocytes, the TRIM-NHL RNA-binding protein LIN-41 is a key component of a large translational regulatory RNP complex that associates with more than 1000 mRNAs (Spike *et al*. 2014b; Tsukamoto *et al*. 2017). Many of these mRNAs encode protein components of LIN-41-containing RNPs and function as translational regulators during oogenesis or early

72   embryonic development. LIN-41 also mediates the 3'-untranslated region (UTR)-mediated

73   translational repression of some of the transcripts that associate with LIN-41 in oocytes and has

74   an essential function to promote the extended meiotic prophase of oocytes (Spike *et al*. 2014a,b;

75   Tsukamoto *et al*. 2017). *lin-41* null mutants are sterile because they produce pachytene-stage

76   oocytes that exit meiotic prophase prematurely; these oocytes inappropriately disassemble the

77   synaptonemal complex, cellularize, activate the CDK-1/cyclin B cyclin-dependent kinase, and

78   enter M phase (Spike *et al*. 2014a). Hypomorphic *lin-41* mutant alleles reduce oocyte quality and

79   cause nondisjunction during female meiosis (Spike *et al*. 2014a). LIN-41 prevents the premature

80   activation of the CDK-1/cyclin B during early oogenesis, in part, through the 3'UTR-mediated

81   translational repression of the CDC-25.3 phosphatase, a CDK-1 activator (Spike *et al*. 2014a,b).

82   Premature CDK-1 activation in *lin-41* mutant oocytes drives precocious M-phase entry and

83   causes oocytes to abnormally transcribe and express genes that are normally expressed

84   zygotically after the OET (Allen *et al*. 2014; Spike *et al*. 2014a; Tocchini *et al*. 2014; Matsuura

85   *et al.* 2016). Thus, a major function of LIN-41 appears to be to preserve mRNAs that are

86   maternally inherited and translationally activated late in oogenesis or during early embryonic

87   development. Many LIN-41-associated transcripts are translated only after LIN-41 is inactivated

88   and degraded via ubiquitin-mediated degradation upon the onset of meiotic maturation (Spike *et*

89   *al*. 2018). For example, LIN-41 associates with and represses the translation of the ORC-1

90   subunit of the origin recognition complex during meiotic prophase, and its degradation permits

91   ORC-1 expression for DNA replication in the embryo (Tsukamoto *et al*. 2017).

92   LIN-41 is highly conserved and its mammalian ortholog, LIN-41/TRIM71, is required for

93   embryonic viability and neural tube closure in mice (Maller Schulman *et al*. 2008; Chen *et al*.

94   2012; Cuevas *et al*. 2015; Mitschka *et al*. 2015). This defect appears to be related to a

95   requirement for LIN-41/TRIM71 for maintaining pluripotency in neural progenitor cells in the

96   embryo. LIN-41/TRIM71 has also been found to promote the pluripotency of embryonic stem

97   cells in the mouse (Chang *et al*. 2012; Worringer *et al*. 2014; Mitschka *et al*. 2015; Liu *et al*.

98   2021). The defects in pluripotency, which underlie the neural tube defects observed in LIN-

99   41/TRIM71 deficient mice, may be highly relevant to the finding of *de novo* heterozygous LIN-

100   41/TRIM71 missense mutations in congenital hydrocephalus cases in humans (Furey *et al*. 2018;

101   Jin *et al*. 2020). Germ cell-specific depletion of LIN-41/TRIM71 in mice causes germ cell loss

102   and sterility in both sexes (Torres-Fernández *et al*. 2021a). Interestingly, male mice with LIN-

103   41/TRIM71-deficient germ cells exhibit a Sertoli cell-only phenotype, which resembles the

104   infertility phenotype of human males with heterozygous LIN-41/TRIM71 mutations (Torres-

105   Fernández *et al*. 2021a). The essential role of LIN-41/TRIM71 in female germ cells remains to

106   be more fully explored. Thus, in mammals, LIN-41/TRIM71 mutations produce distinct

107   phenotypes in germ cells and somatic cells, which highlights the flexibility of LIN-41/TRIM71

108   proteins for deployment in developmental cell fate decisions. Indeed, LIN-41 was first

109   discovered as a target of the *let-7* microRNA in the genetic pathway controlling the

110   developmental timing of somatic cells in *C. elegans* (Reinhart *et al*. 2000; Slack *et al*. 2000). The

111   regulation of LIN-41/TRIM71 orthologs by *let-7* microRNAs appears to be highly conserved in

112   animals (O'Farrell *et al*. 2008; Kloosterman *et al*. 2004; Kanamoto *et al*. 2006; Lin *et al*. 2007;

113   Rybak *et al*. 2009; Worringer *et al*. 2014). This mode of regulation is not observed in the *C.*

114   *elegans* germline, as the *let-7* microRNA appears to be only expressed in somatic cells (Lau *et*

115   *al*. 2001). A new twist is that recent studies suggest that mammalian LIN-41/TRIM71 can inhibit

116   the accumulation of *let-7* microRNAs (Liu *et al*. 2021; Torres-Fernández *et al*. 2021b),

117   suggesting its involvement as a component of a bistable developmental switch. Although it is not

7

118   known whether LIN-41 can inhibit the *let-7* pathway in *C. elegans*, it is clear that LIN-41 is a

119   component of a bistable switch regulating oocyte meiotic maturation in this organism—LIN-41

120   inhibits CDK-1 activation, and in turn, active CDK-1 promotes the ubiquitin-mediated

121   degradation of LIN-41 upon the onset of meiotic maturation (Spike *et al*. 2018).

122   The rapid elimination of LIN-41 upon the onset of meiotic maturation is emblematic of

123   the highly choreographed and exquisitely timed patterns of degradation of RNA-binding proteins

124   during late oogenesis and the OET in many organisms (Nishi *et al*. 2005; Stitzel *et al*. 2006;

125   Shirayama *et al*. 2006; Sha *et al.* 2017; Kisielnicka *et al.* 2018; Cao *et al*. 2020, 2021; Zavortink

126   *et al*. 2020; reviewed by Robertson and Lin 2015). Previous results suggested that an SCF-type

127   E3 ubiquitin ligase containing the FBW7/Cdc4 ortholog SEL-10 promotes the degradation of

128   LIN-41 using a bi-partite degron located near the N-terminus of LIN-41 (Spike *et al.* 2018). The

129   ubiquitin proteasome pathway utilizes an E1-E2-E3 enzymatic relay to transfer ubiquitin to mark

130   proteins for degradation by the 26S proteasome. E3 ubiquitin ligases, comprising multi-subunit

131   enzymes or single chain proteins, function as substrate specificity factors to conjugate multiple

132   ubiquitin moieties to target proteins. SEL-10 is a highly conserved and well-studied substrate-

133   recognition subunit (Hubbard *et al*. 1997, de la Cova and Greenwald 2012). After substrate

134   proteins are recognized and ubiquitinated, they are received by the 19S regulatory particles of the

135   proteasome, which bind the ubiquitin chains, unfold the substrate, and processively translocate it

136   into the 20S particle for degradation (reviewed by Finley 2009; Collins and Goldberg 2017).

137   In this work, we strengthen our understanding of LIN-41 degradation and begin to

138   investigate how additional RNA-binding proteins in LIN-41 RNPs are degraded upon the onset

139   of meiotic maturation. First, we show that SEL-10 is expressed in oocytes and use

140   photoconversion of DENDRA::LIN-41 in maturing oocytes to demonstrate unequivocally that

141   SEL-10 is required to degrade LIN-41 during the OET. Next, we identify the Pumilio/FBF-

142   family RNA-binding proteins PUF-3 and PUF-11 as proteins that are degraded soon after

143   meiotic maturation. PUF-3 and PUF-11 are components of LIN-41-containing RNPs in oocytes

144   (Tsukamoto *et al*. 2017) that are 89 percent identical at the amino acid level and play important

145   roles in germline stem cell and embryonic development (Hubstenberger *et al.* 2012, Haupt *et al.*

146   2020). Although both PUF-3 and PUF-11 are degraded soon after meiotic maturation in a CDK-

147   1-dependent fashion, the degradation of both proteins occurs independently of SEL-10.

148   Collectively, these results indicate that PUF-3 and PUF-11 are not degraded as a consequence of

149   LIN-41 degradation and that LIN-41 RNPs are dismantled in a concerted fashion during the

150   OET. Finally, we find that several different GFP-tagged fusion proteins that are degraded during

151   the OET, including fusions with PUF-3, PUF-11 and LIN-41, are incompletely degraded when

152   the function of the conserved ETC-1/UBE3C/Hul5 HECT-domain ubiquitin ligase is abrogated,

153   indicating that ETC-1 is important for proteasome processivity. We provide evidence that the

154   GFP tag causes this proteolysis defect, re-evaluate key aspects of a previous report that assigned

155   a different role to ETC-1 (Wang *et al*. 2013), and propose that proteasomal processivity is

156   critical for the rapid and efficient targeting of a plethora of oocyte regulatory proteins for

157   degradation during the OET.

158

159 **MATERIALS AND METHODS**

160 *Strains*

161 The genotypes of strains used in this study are reported in Table S1. The following mutations

162 were used: LGI—*rnp-8(tn1860[rnp-8::gfp::tev::3xflag])*, *mat-1(ax161*ts*)*, *lin-*

163 *41(tn1541[gfp::tev::s::lin-41]))*, *lin-41(tn1892[mscarlet::tev::3xflag:lin-41])*, *lin-*

164 *41(tn1894[dendra::tev::3xflag::lin-41])*, *lin-41(tn2054[gfp::tev::3xflag::lin-41])*, *lin-*

165 *41(tn2055[gfp::tev::3xflag::lin-41])*, and *fog-3(q443)*. *lin-41(tn2054)* and *lin-41(tn2055)* were

166 generated independently but are identical at the DNA sequence level. LGII—*etc-1(gk5182)*, *etc-*

167 *1(tn1919[gfp::tev::3xflag::etc-1])*, *etc-1(tn1920[gfp::tev::3xflag::etc-1])*, and *unc-4(e120)*.

168 LGIII—*plk-1(or683*ts*)*, *emb-30(tn377*ts*)*, and *cul-2(or209*ts*)*. LGIV—*puf-11(tn1824[puf-*

169 *11:gfp::tev::3xflag])*, *puf-11(q971)*, *cyb-1(tn1806[cyb-1::gfp::tev::3xflag])*, *unc-22(e66)*, *puf-*

170 *3(tn1820[puf-3::gfp::tev::3xflag])*, and *puf-3(q966)*. LGV—*lon-3(e2175)*, *sel-10(ar41)*, *sel-*

171 *10(ok1632)*, *sel-10(tn1816[sel-10::gfp::tev::3xflag])*, *sel-10(tn1817[sel-10::gfp::tev::3xflag])*,

172 *sel-10(tn1875[gfp::tev::3xflag::sel-10])* and *fog-2(oz40)*. *sel-10(tn1816)* and *sel-10(tn1817)*

173 were generated independently but are identical at the DNA sequence level. The following

174 balancers were used: *tmC18[dpy-5(tm1236)]* I (Dejima *et al.* 2018), *mnC1[dpy-10(e128) unc-*

175 *52(e444) umnIs32]* II, *nT1[qIs51]* (IV; V). The following transgene insertions were used:

176 *itIs37[pie-1p::mcherry::histoneH2B::pie-1 3'UTR, unc-119(+)]* IV (McNally *et al.* 2006) and

177 *ddIs128[ify-1::2xty1::egfp::3xflag(92C12) + unc-119(+)]* (Sarov *et al.* 2012).

178 *mScarlet and Dendra repair templates*

179 The repair templates used to create *lin-41(tn1892[mscarlet::tev::3xflag::lin-41])* and *lin-*

180 *41(tn1894[dendra::tev::flag::lin-41])* were generated by Gibson assembly using the NEBuilder

10

181   HiFi DNA Assembly master mix (New England Biolabs, Ipswich, MA) and five different PCR

182   products: (1) a *lin-41* 5' homology arm (~0.6 kb), (2) a codon-optimized mScarlet-I or a Dendra

183   coding sequence with introns (~0.9 kb), (3) self-excising cassette (SEC)-containing sequences

184   (~5.7 kb), (4) a *lin-41* 3' homology arm (~0.8 kb), and (5) vector backbone sequences (~2.6 kb).

185   *lin-41* homology arms (1 and 4) were amplified from genomic DNA prepared from the wild type.

186   SEC and vector sequences (3 and 5) were amplified from *Cla*I and *Spe*I-digested pDD268

187   plasmid DNA (Dickinson *et al*. 2015). mScarlet-I and Dendra were amplified from the plasmids

188   pMS050 (Addgene plasmid #91826), a gift from Bob Goldstein, and pEG545 (Griffin *et al*.

189   2011), a gift from Geraldine Seydoux. Primer sequences are presented in File S1. All PCR

190   products were initially column purified (Qiagen, Valencia, CA) and most of the plasmids

191   recovered after assembly lacked the SEC fragment; only 10% and 5% of the mScarlet-I and

192   Dendra repair constructs were complete, respectively. While making different *lin-41* repair

193   constructs using the same method and many of the same PCR fragments, we found that gel

194   purifying the SEC PCR product increased the inclusion of the SEC fragment to 80% of the

195   assembled plasmids.

196   Constructs created by Griffin *et al*. (2011) that contain DENDRA-expressing sequences

197   optimized for use in *C. elegans* (Gallo *et al*. 2010) are annotated in Addgene as containing

198   DENDRA2 (e.g., pEG545, Addgene plasmid #40116 and pEG345, Addgene plasmid #40077).

199   DENDRA2 is a modified form of DENDRA that has an important single amino acid change near

200   the C-terminus (A224V) as well as a 5-amino acid insertion near the N-terminus (Gurskaya *et al*.

201   2006; Chudakov *et al*. 2007). The relationship between DENDRA and DENDRA2 is most easily

202   visualized using the fluorescent protein database www.fpbase.org (Lambert 2019). We

203   sequenced the pEG545 plasmid and confirmed that it encodes DENDRA; the DENDRA-coding

11

204   sequence lacks both the A224V amino acid change and the 5-amino acid insertion found in

205   DENDRA2. Since we obtained pEG545 directly from the Seydoux lab, we also analyzed the

206   Addgene-deposited sequences of pEG545 and pEG345. Although those sequences are

207   incomplete, they confirm that each plasmid encodes DENDRA[A224]. As both plasmids have

208   been used to generate many different fusion proteins labeled as containing DENDRA2 [e.g.,

209   Herrera *et al.* (2016) and Rosu and Orna Cohen-Fix (2017)], this annotation error may be

210   relatively common in the *C. elegans* literature.

211   ***Genome editing***

212   Plasmids that express guide RNAs (gRNAs) under the control of the U6 promoter were

213   generated as described (Arribere *et al*. 2014). Repair templates used to tag genes with *gfp* were

214   also generated as described (Dickinson *et al.* 2015). Repair templates used to tag genes with

215   mSCARLET-I and DENDRA were generated as described in the previous section. Genome

216   editing was performed by injecting wild-type adult gonads with a DNA mix containing a repair

217   template (10 ng/μl), one or more gRNA plasmids (25 ng/μl each), Cas9-expressing plasmid

218   (pDD162, 50 ng/μl), and injection marker (pMyo2::Tdtomato, 4 ng/μl) and selecting for repairs

219   and selection cassette excisions using standard methods (Dickinson *et al*. 2015). Null mutations

220   in *lin-41* are both Dumpy (Dpy) and sterile (Slack *et al.* 2000; Spike *et al.* 2014a). None of the

221   animals homozygous for the *mScarlet^SEC^lin-41, Dendra^SEC^lin-41* and *GFP^SEC^lin-41*

222   repairs were Dpy, but some were sterile, consistent with the interpretation that the insertion of

223   each SEC (self-excising cassette) at the 5' end of the *lin-41* gene created reduction-of-function

224   rather than null alleles of *lin-41*. Each *lin-41* repair was balanced with *tmC18* and the SEC was

225   removed from the *lin-41* locus in balanced heterozygotes. Fluorescently tagged *lin-41* alleles

226   were homozygous fertile after SEC excision. All edited loci were validated by sequencing the

12

227   repair junctions using PCR products as templates. At least two alleles derived from

228   independently injected parents were isolated and assigned allele names; all alleles are available

229   upon request.

230   *Antibody staining*

231   Dissected gonads stained with the rabbit anti-GLD-1 primary antibody (1:200 or 1:300 dilution;

232   Jan *et al*. 1999) were fixed in 1% paraformaldehyde for 10 min, with a 5-min post fix step in ice-

233   cold methanol as previously described (Rose *et al.* 1997; Spike *et al.* 2018). Primary antibodies

234   were detected using Cy3-conjugated donkey anti-rabbit secondary antibodies (1:500 dilution;

235   Jackson ImmunoResearch, West Grove, PA).

236   *Microscopy and image analysis*

237   Microscope images in Figures 4 and S2 were acquired on a Carl Zeiss motorized Axioplan 2

238   microscope with a 63x Plan-Apochromat (numerical aperture 1.4) objective lens using an

239   AxioCam MRm camera and AxioVision software (Carl Zeiss, Thornwood, NY). Microscope

240   images in Figures 5I-L, S6A-F and S7 were acquired on a Nikon Ni-E microscope with either a

241   Plan Apo λ 60x (numerical aperture 1.4) objective or a Plan Fluor 40x Oil (numerical aperture

242   1.3) objective using NIS elements (Nikon Inc., Melville, NY). All the remaining microscope

243   images were acquired on a Nikon Ti2 inverted confocal microscope with a Plan ApoIR 60x

244   objective (numerical aperture 1.27), motorized stage and Galvano scanner using NIS elements

245   (Nikon Inc., Melville, NY). When using the Nikon Ti2 microscope, the large image function of

246   NIS elements was used to acquire images that show the entire germline. We quantified the

247   average fluorescence intensity in selected areas of images using the measure function of ImageJ

248   (Schneider *et al.* 2012). Each measurement was background corrected using the average

13

249   fluorescence intensity of a nearby area outside the body of the worm. Multiple images were

250   analyzed per genotype, as specified in the text.

251   ***Photoconverting ^{Green}DENDRA::LIN-41 to ^{Red}DENDRA::LIN-41***

252   Worms were mounted without anesthetic on 10% agarose pads in a 1:1 solution of M9 buffer and

253   0.1 μM polystyrene beads (Polysciences, Inc., Warrington, PA) essentially as described (Rosu

254   and Cohen-Fix 2020). Photoactivation and imaging was performed using the Nikon Ti2 inverted

255   confocal microscope equipped as described in the previous section. A region of interest

256   encompassing the −1 oocyte was selected for photoactivation using the 405 nm laser at 10%

257   power for 31.25 seconds (125 loops at 4 frames per second) and a large pinhole (173.69 microns)

258   to promote DENDRA photoconversion throughout the oocyte. After photoactivation, animals

259   were allowed to recover on NGM plates seeded with OP50-1 bacteria for either 60 min or 100

260   min and then mounted a second time. Confocal settings optimized to image oocytes after

261   photoconversion were used to collect images of the ^{Green}DENDRA::LIN-41 and

262   ^{Red}DENDRA::LIN-41 in oocytes and embryos at all stages of the experiment: before

263   photoactivation, after photoactivation, and after recovery.

264   Although the conditions used for photoactivation were generally compatible with oocyte

265   meiotic maturation and ovulation, our experimental manipulations sometimes interfered with

266   these events. For example, one *lin-41(tn1894)* animal failed to move after recovery, suggesting

267   that it might have been damaged while mounting on or recovering from the agarose pad.

268   ^{Red}DENDRA::LIN-41 was still detectable in the −1 and −2 oocytes of the photoconverted arm

269   after a 100-min recovery period, indicating that the converted oocytes in this damaged animal

270   had not matured or ovulated. The other *lin-41(tn1894)* animals (n=5) survived the experimental

14

271 manipulations and exhibited exclusively green oocytes in the −1 and −2 positions in each

272 photoconverted arm (n=6 arms, the −1 oocytes of both arms were converted in one animal),

273 confirming that oocytes had matured and been ovulated into the uterus during the recovery

274 period (60 min (n=2) or 100 min (n=4)). All *lin-41(tn1894); sel-10(ok1632)* animals survived

275 our experimental manipulations (n=4 animals), and most of the photoconverted arms had

276 exclusively green oocytes in the −1 and −2 positions (n=4/5 arms, the −1 oocytes of both arms

277 were converted in one animal) and one or two red embryos in the uterus after the recovery

278 period. The sole exception was in an animal that laid only 2 eggs during the 100-min recovery

279 period and appeared to be sickly. This animal had a bright red 1-cell stage embryo in the +1

280 position and a fainter red oocyte in the −1 position. The −1 oocyte converted in this gonad arm

281 must have experienced a substantial temporal delay prior to oocyte maturation and ovulation, as

282 a shorter (60 min) recovery period was sufficient for two ovulation events in the healthier *lin-*

283 *41(tn1894); sel-10(ok1632)* animals.

284 ***itIs37 puf-3(tn1820) and puf-11(tn1824) puf-3(tn1820) double mutants***

285 Crosses with *puf-11(tn1824)* and *puf-3(tn1820)* established that the *itIs37[pie-*

286 *1p::mcherry::histoneH2B::pie-1 3'UTR, unc-119(+)]* insertion on chromosome IV is tightly

287 linked to *puf-11* and more loosely linked to *puf-3*. 0 of 72 progeny from *itIs37 + / + puf-*

288 *11(tn1824)* parents carried a recombinant *itIs37 puf-11(tn1824)* chromosome, while 5 of 64

289 progeny from *itIs37 + / + puf-3(tn1820)* parents carried a recombinant *itIs37 puf-3(tn1820)*

290 chromosome. Together, these observations suggested that *itIs37* is ~7.8 map units to the left of

291 *puf-3*, in good agreement with the relative genetic positions of *puf-11* and *puf-3* described in

292 WormBase (http://www.wormbase.org, release WS278; Harris *et al*. 2014). We utilized *unc-*

15

293   *22(e66)*, which causes a homozygous Uncoordinated (Unc) phenotype and is located in-between

294   *puf-11* and *puf-3*, to construct the *puf-11(tn1824) puf-3(tn1820)* double mutant. Animals carrying

295   *itIs37 puf-3(tn1820)* and *puf-11(tn1824) unc-22(e66)* recombinant chromosomes were mated

296   with each other. Animals with one copy of each chromosome were selected and allowed to self-

297   fertilize. In the next generation, non-Unc-22 animals were examined for *itIs37*-derived

298   mCHERRY::HISTONE expression using fluorescence microscopy. A single *itIs37*-negative

299   animal was identified among the 168 non-Unc animals examined, and this animal segregated

300   approximately one quarter Unc progeny in the next generation. Based on the mapping data, we

301   anticipated that this rare animal carried either a *puf-11(tn1824) puf-3(tn1820)* or a *puf-11(+) puf-*

302   *3(tn1820)* recombinant chromosome in *trans* to the parental *puf-11(tn1824) unc-22(e66)*

303   chromosome. Animals homozygous for the recombinant chromosome were analyzed using

304   primers that produce allele-specific PCR products (File S1) and found to carry both *puf-*

305   *11(tn1824)* and *puf-3(tn1820)*.

306   **RNA interference**

307   Gene-specific RNA interference (RNAi) was performed by feeding *C. elegans* with double-

308   stranded RNA (dsRNA)-expressing *E. coli* (Timmons and Fire 1998) at 22 °C using the RNAi

309   culture media described by Govindan *et al*. (2006). RNAi clones were obtained from Source

310   BioScience (Nottingham, UK), and the identities of important RNAi clones were verified by

311   DNA sequencing (see File S1 for details). Exposure to dsRNA-expressing *E. coli* was initiated

312   during the fourth larval stage and animals were examined and imaged after 2 days. Under these

313   RNAi conditions and at the time-point analyzed, all *cdk-1(RNAi)* animals produced arrested 1-

314   cell embryos and therefore had a strong *cdk-1(RNAi)* phenotype (see Boxem *et al.* 1999). Using

315   the same RNAi conditions, the gonad arms of *wee-1.3(RNAi)* animals exhibited a range of oocyte

16

316   phenotypes. Gonads with a mild *wee-1.3(RNAi)* phenotype have relatively large and normal-

317   appearing oocytes that occupy approximately normal positions with respect to each other and to

318   the spermatheca. Gonads with strong *wee-1.3(RNAi)* phenotype have small, sometimes indistinct

319   oocytes or a mass of oocyte-like material near the spermatheca. Burrows *et al.* (2006) also noted

320   that prolonged RNAi results in small oocytes, consistent with the idea that this phenotype is

321   caused by a strong response to *wee-1.3(RNAi)*. GFP$_S$::LIN-41 is prematurely degraded in animals

322   with both weak and strong *wee-1.3(RNAi)* phenotypes (Spike *et al.* 2014a, 2018). In the screen

323   for E3 ubiquitin ligases that degrade PUF-3::GFP, we did not exclusively use RNAi to test the

324   SCF subunit CUL-2. Since our *cul-2(RNAi)* clone does not trigger a good RNAi response (Spike

325   *et al.* 2018), we also examined *cul-2(or209*ts*)*; *puf-3(tn1820[puf-3::gfp::tev::3xflag])* adults 1

326   day after they were upshifted to 25 °C as L4-stage larvae. All other ubiquitin ligase subunits

327   were screened using RNA interference alone.

328   ***Western blots***

329   Each lane was loaded with a protein lysate made from adult worms picked into 10 microliters of

330   phosphate-buffered saline (PBS) containing proteinase inhibitors (2x complete EDTA-free;

331   Millipore-Sigma, St. Louis, MO). Whole-worm lysates were frozen at –80 °C and prepared for

332   electrophoresis by adding LDS sample buffer supplemented with a reducing agent (Invitrogen,

333   Carlsbad, CA). Immediately after adding the sample buffer, the samples were heated at 70 °C

334   and vortexed multiple times prior to loading on a gel. Lysates were made from 40 Day 1 adult

335   worms (24 hours past the L4 stage at 20 °C) with a few exceptions. Some lysates expressing

336   CYB-1::GFP were made from 50 instead of 40 worms (hermaphrodites in Figures 7A and S5B;

337   males in Figures 7B and S5D). In addition, the mated females used for lysates were not

338   developmentally staged (Figure S5C). Instead, gravid females were selected from mixed-stage

17

339 plates. Proteins were separated using 3–8% Tris-Acetate gels (Invitrogen, Carlsbad, CA) and

340 visualized after western blotting. Blots were blocked with 5% nonfat dried milk. The primary

341 antibodies used were mouse anti-FLAG M2 (Millipore-Sigma) at a 1:2,000–1:4,000 dilution and

342 rabbit anti-GFP NB600-308 (Novus Biologicals, Littleton, CO) at a 1:4,000 dilution. The

343 secondary antibodies used were peroxidase-conjugated goat anti-mouse (Thermo Scientific,

344 Waltham, MA) at a 1:30,000 dilution or peroxidase-conjugated donkey anti-rabbit (Thermo

345 Scientific) at a 1:5,000 dilution. Detection was performed using SuperSignal West Femto

346 Maximum Sensitivity Substrate and CL-XPosure film (Thermo Scientific).

347 *eGFP, mSCARLET-I and DENDRA fusion protein tag sequences*

348 The predicted amino sequence and molecular mass of each protein tag is presented in File S2 for

349 reference. All GFP tags express the GFP[S65C] enhanced GFP variant commonly used in *C.*

350 *elegans* (Green *et al.* 2008). Most also contain the apparently neutral GFP[Q80R] change likely

351 introduced into the original GFP cDNA sequence by PCR error (Tsien 1998).

352 *Data availability*

353 All alleles and strains (Table S1), plasmids (File S1) and Sanger sequencing files are available

354 upon request. Primer sequences are provided in File S1. File S2 contains the amino acid

355 sequences of fluorophore tags used in this work. Supplemental materials are available at

356 Figshare: https://doi.org/

357

358 ## RESULTS AND DISCUSSION

359 ### *SEL-10 is present in the cytoplasm and nucleoplasm of oogenic germ cells*

360 SEL-10/Cdc4/FBW7 is a highly conserved F-box protein; it is the substrate-recognition subunit

361 of a Skp, Cullin, F-box (SCF)-containing E3 ubiquitin ligase complex that promotes the

362 ubiquitination and degradation of specific substrates (reviewed in Deshaies and Ferrell 2001;

363 Welcker and Clurman 2008). In *C. elegans*, SEL-10 functions in the oogenic germline and

364 during the OET to promote the timely elimination of the cytoplasmic RNA-binding proteins

365 GLD-1 and LIN-41 at different stages of oogenesis (Kisielnicka *et al*. 2018; Spike *et al.* 2018).

366 Consistent with this idea, *sel-10* mRNA is expressed throughout the oogenic germlines of adult

367 hermaphrodites and the *sel-10* 3' UTR is permissive for the translation of green fluorescent

368 protein (GFP) in pre-meiotic and meiotic cells during oogenesis (Kisielnicka *et al.* 2018).

369 However, the expression of SEL-10 has not been reported in oocytes or in any other region of the

370 *C. elegans* germline, possibly because SEL-10 expression constructs were examined in the

371 context of extrachromosomal arrays (Ding *et al.* 2007; Dorfman *et al.* 2009), which can silence

372 the expression of germline genes in *C. elegans* (Kelly *et al.* 1997). To avoid this technical issue,

373 we used genome editing to generate new alleles of *sel-10* that have a GFP-tag fused to the SEL-

374 10 protein at both the amino-terminus (N-terminus, GFP_F::SEL-10 in Figure 1) and carboxyl-

375 terminus (C-terminus, SEL-10::GFP_F in Figure 1). In the figures, and where needed for textual

376 clarity, we will indicate the presence and relative position of a 3xFLAG or an S epitope tag in a

377 fusion protein with an F or S subscript, respectively. The alleles that express GFP::SEL-10, SEL-

378 10::GFP, and many of the other fusion proteins used in this work, are shown in Figure S1.

379   The pattern of GFP expression from each *sel-10* allele confirms that SEL-10 is expressed

380   throughout the oogenic germline of adult hermaphrodites and in early embryos (Figure 1, C and

381   E). GFP::SEL-10 and SEL-10::GFP are present in the nucleoplasm and cytoplasm of oocytes and

382   distal germ cells, but show slightly different patterns of localization. GFP::SEL-10 is enriched in

383   the nucleoplasm relative to the cytoplasm at all stages of germ cell development (Figure 1C).

384   SEL-10::GFP is present at similar levels in the nucleoplasm and cytoplasm of distal germ cells

385   and becomes enriched in the nucleoplasm of growing oocytes (Figure 1E). Using confocal

386   images collected with identical settings, we measured 23% and 43% increases in background-

387   corrected cytoplasmic fluorescence in the rachis and the −3 oocyte, respectively, in SEL-10::GFP

388   animals relative to GFP::SEL-10 animals ($P<0.01$, n=7 images per genotype). However, nuclear

389   fluorescence in the −3 oocyte of each strain was not significantly different ($P>0.1$). We conclude

390   that, at least in the oogenic germline, SEL-10::GFP appears to be more abundant than GFP::SEL-

391   10 and more likely to reside in the cytoplasm.

392   The different patterns of GFP::SEL-10 and SEL-10::GFP localization might reflect the

393   disruption or alteration of SEL-10 function by the inserted protein tags. We examined the

394   accumulation of LIN-41 and GLD-1 in animals homozygous for each GFP-tagged allele of *sel-*

395   *10* to address this possibility. LIN-41 was monitored using *lin-41(tn1892[mscarlet::3xflag::lin-*

396   *41])*, a new allele of *lin-41* that produces a fusion protein with an mSCARLET-tag fused to the

397   N-terminus of LIN-41 (Figure S1B; mSC$_F$::LIN-41). Endogenous GLD-1 levels were analyzed

398   by immunostaining. mSCARLET::LIN-41 is strongly expressed in wild-type and *sel-10(ok1632)*

399   loss-of-function mutant oocytes (Figure 1, A and B). mSCARLET::LIN-41 is down-regulated in

400   wild-type embryos (Figure 1A), but persists at elevated levels in the embryos produced by *sel-*

401   *10(ok1632)* mutant animals (Figure 1B). The downregulation of mSCARLET::LIN-41 protein

402   expression during the OET is therefore SEL-10-dependent, as described for endogenous LIN-41

403   and a GFP-tagged LIN-41 fusion protein (Figure S1B; GFP$_S$::LIN-41; Spike *et al*. 2018).

404   mSCARLET::LIN-41 is downregulated in the embryos of GFP::SEL-10-expressing animals (*sel-*

405   *10(tn1875)*, Figure 1D), but persists at elevated levels in the embryos of SEL-10::GFP-

406   expressing animals (*sel-10(tn1817)*, Figure 1F). Similar results were observed with GLD-1

407   (Figure S2). GLD-1 is downregulated as developing oocytes exit pachytene near the loop region

408   (Figure S2, A and C), and this process is impaired in *sel-10(lf)* mutants, resulting in elevated

409   levels of GLD-1 in proximal oocytes (Kisielnicka *et al.* 2018; Spike *et al.* 2018). GLD-1 is

410   downregulated in the oocytes of GFP::SEL-10-expressing animals (*sel-10(tn1875)*, Figure S2B),

411   but persists at elevated levels in the oocytes of SEL-10::GFP-expressing animals (*sel-10(tn1816)*,

412   Figure S2D). We conclude that at least two of the normal functions of SEL-10 are compatible

413   with the insertion of a GFP tag at the N-terminus of SEL-10 but are disrupted by the insertion of

414   a GFP tag at the SEL-10 C-terminus. Furthermore, these observations suggest that the

415   nucleoplasm-enriched localization pattern of GFP::SEL-10 shown in Figure 1C likely represents

416   the correct localization pattern of SEL-10 in the oogenic germline. Although known targets of

417   SEL-10 in the *C. elegans* germline are predominantly cytoplasmic (e.g., LIN-41, GLD-1 and

418   CPB-3 (Kisielnicka *et al.* 2018; Spike *et al.* 2018)), orthologs of SEL-10 are present in the

419   nucleoplasm in *S. cerevisiae* (Cdc4p) (Choi *et al.* 1990) and in both the nucleoplasm and

420   cytoplasm in humans (FBW7α and FBW7β isoforms, respectively) (Welcker *et al.* 2004).

421

422

423

SEL-10 is required to degrade LIN-41 during the OET

LIN-41 disappears rapidly upon the onset of meiotic maturation. We previously

hypothesized that LIN-41 is phosphorylated at this stage and recognized by a SEL-10-containing

E3 ubiquitin ligase that targets LIN-41 for proteolysis (Spike *et al*. 2018). To confirm that SEL-

10 promotes the degradation of LIN-41 during the OET, we generated *lin-*

41(tn1894[dendra::3xflag::lin-41]), a new allele of *lin-41* that produces a protein with a

DENDRA-tag fused to the LIN-41 N-terminus (Figure S1B; DND$_F$::LIN-41) and crossed it into

a *sel-10(ok1632)* mutant background. Photoactivation irreversibly converts the fluorescence

emitted by DENDRA from green to red (^{Green}DENDRA and ^{Red}DENDRA, respectively)

(Gurskaya *et al*. 2006). The ^{Green}DENDRA::LIN-41 present in the −1 oocytes of *sel-10(ok1632)*

and *sel-10(+)* animals was targeted for conversion to ^{Red}DENDRA::LIN-41 using a 405 nm

laser. Robust photoconversion was observed in the −1 oocyte, with a small amount of red

fluorescence sometimes visible in the adjacent cytoplasm of the −2 oocyte (Figure 2, A, B, F,

and G). After a suitable recovery period to permit oocyte maturation, ovulation, and some

embryonic development, bright ^{Red}DENDRA::LIN-41 was evident in a single embryo in the

uterus of *sel-10(ok1632)* animals (Figure 2, C–E; n=5/5). In general, we noted that the next-

youngest embryo (or −1 oocyte in one animal, see Materials and Methods) also contained

^{Red}DENDRA::LIN-41 (n=4/5), but at a much lower level. We did not observe bright

^{Red}DENDRA::LIN-41 in any of the embryos in the uteri of *sel-10(+)* animals (n=6), although we

sometimes saw an embryo with a slight haze of red fluorescence that we hypothesized might be

derived from the converted ^{Red}DENDRA::LIN-41 −1 oocyte (Figure 2, H and I). Relative to

these *sel-10(+)* embryos, we measured a 6- to 10-fold higher level of background-corrected

^{Red}DENDRA::LIN-41 fluorescence in the brightest *sel-10(ok1632)* embryos (n=4 of each

447   genotype). Together, these results indicate that the fluorescently tagged [Red]DENDRA::LIN-41

448   observed in *sel-10(ok1632)* embryos originates in oocytes and confirm that LIN-41 is degraded

449   during the OET in wild-type animals.

450

451   ***PUF-3 and PUF-11 are degraded during the OET***

452   PUF-3 and PUF-11 are nearly identical Pumilio-family RNA-binding proteins that function

453   redundantly with respect to normal embryonic development in *C. elegans* (Hubstenberger *et al.*

454   2012; Haupt *et al.* 2020). PUF-3 and PUF-11 proteins and mRNAs co-purify with LIN-41-

455   containing ribonucleoprotein (RNP) complexes (Tsukamoto *et al.* 2017). Furthermore, LIN-41

456   and PUF-3/11 were each identified as factors important for the 3'UTR-mediated translational

457   repression of the Rbfox-related RNA-binding protein SPN-4 in oocytes (Hubstenberger *et al.*

458   2012; Tsukamoto *et al*. 2017). These observations suggest that LIN-41, PUF-3, and PUF-11

459   function together in developing oocytes. We confirmed that PUF-3 and PUF-11 are expressed in

460   oocytes, as described (Haupt *et al.* 2020), and also examined the expression patterns of PUF-3

461   and PUF-11 during the oocyte-to-embryo transition. We created new alleles of *puf-3* and *puf-11*

462   that fuse a GFP-tag to the C-terminus of each PUF protein (Figure S1C; PUF-3::GFP$_F$ and PUF-

463   11::GFP$_F$) and found that PUF-3 and PUF-11 are eliminated during the OET in a manner that

464   resembles LIN-41 (Figure 3). PUF-3::GFP and PUF-11::GFP are abundant in oocytes, but the

465   expression of each protein is strongly diminished soon after oocyte meiotic maturation and

466   ovulation (Figure 3, A and D; Figure S3, A and B). Consequently, PUF-3::GFP and PUF-

467   11::GFP expression appear to be largely absent from embryos (Figure 3A) or limited to a single

468   young embryo (Figure 3D and Figure S3, A and B). A similar pattern is observed with

23

469   GFP::LIN-41 and mSCARLET::LIN-41 (Spike *et al.* 2018; Figure 1A). Moreover, PUF-3::GFP

470   or PUF-11::GFP and mSCARLET::LIN-41 identify the same young embryos (if present, as in

471   Figure 3, D and E; n≥7 animals of each genotype imaged as shown). To determine when PUF-3

472   is eliminated from embryos, we examined PUF-3::GFP in oocytes and embryos that express an

473   mCHERRY::HISTONE fusion protein. Relative to the adjacent −1 oocyte, PUF-3::GFP levels

474   are substantially reduced in meiotic embryos that are in metaphase I (Figure 3, G–J) and most

475   PUF-3::GFP appears to be eliminated by the end of the first meiotic division (Figure 3K). This

476   roughly corresponds to the time window during which LIN-41 is degraded; time-lapse imaging

477   previously demonstrated that GFP::LIN-41 is dramatically reduced by the end of the first meiotic

478   division (Spike *et al.* 2018).

479   While LIN-41, PUF-3 and PUF-11 are strongly reduced soon after meiotic maturation

480   and ovulation, each protein has a distinct pattern of expression in the adult germline (Figure 3,

481   A–F). For example, the accumulation of PUF-3::GFP and PUF-11::GFP appears to peak at a

482   later stage of oogenesis than mSCARLET::LIN-41 (Figure 3, C and F). In addition, PUF-

483   11::GFP is distinctly more abundant than PUF-3::GFP in the distal germline (compare Figure 3,

484   A and D). Haupt *et al.* (2020) also observed higher levels of PUF-11 in the distal germline using

485   alleles that express V5 epitope-tagged PUF-3 and PUF-11 proteins. We screened for and

486   identified a recombinant that expresses both PUF-3::GFP and PUF-11::GFP using standard

487   genetic methods (see Materials and Methods). As expected from the individual expression

488   patterns, GFP expression was higher in the oocytes of these animals [*puf-11(tn1824) puf-*

489   *3(tn1820)* genotype] than in the oocytes of either parent [*puf-11(tn1824)* or *puf-3(tn1820)* alone],

490   and the level of GFP expression in the distal germline was similar to the PUF-11::GFP-

491   expressing strain (Figure S3, A–C). *puf-11(tn1824) puf-3(tn1820)* animals are overtly wild-type;

492   they are homozygous viable and fertile, with a brood size similar to the wild type (333 ± 40

493   larvae, n=15 animals at 20 °C). In addition, most of the embryos produced by *puf-11(tn1824)*

494   *puf-3(tn1820)* animals hatch (~1% embryonic lethality). Since animals that are doubly

495   homozygous for deletion alleles of *puf-11* and *puf-3* [*puf-11(q971) puf-3(q966)* animals] exhibit

496   maternal-effect embryonic lethality (Haupt *et al.* 2020), the GFP-tagged alleles of *puf-11* and

497   *puf-3* must retain some wild-type function. As a more stringent test, we crossed homozygous *puf-*

498   *11(tn1824) puf-3(tn1820)* males to balanced *puf-11(q971) puf-3(q966) / nT1[qIs51]*

499   hermaphrodites to generate *puf-11(tn1824) puf-3(tn1820) / puf-11(q971) puf-3(q966)* animals.

500   Animals with this genotype produced many embryos that were viable (n=25 animals). We

501   conclude that the GFP tag inserted at the C-terminus of PUF-3 and PUF-11 is largely compatible

502   with the function of each protein.

PUF-3 and PUF-11 are degraded in response to active CDK-1

504   LIN-41 is degraded in response to meiotic resumption and the activation of the cyclin-dependent

505   kinase CDK-1 (Spike *et al.* 2014a, 2018). Likewise, we find that using RNA interference (RNAi)

506   to strongly reduce CDK-1 activity causes PUF-3::GFP and PUF-11::GFP to persist in embryos

507   (Figure 4, A and E; n>65 for each PUF::GFP with 100% penetrance). Furthermore, a strong

508   RNAi-mediated reduction in the activity of the WEE-1.3 kinase, a negative regulator of CDK-1

509   (Burrows *et al*. 2006), causes oocytes to downregulate PUF-3::GFP and PUF-11::GFP

510   prematurely (Figure 4, B and F). The latter phenotype was partially penetrant; it was observed in

511   32/46 of the PUF-3::GFP and 25/44 of the PUF-11::GFP-expressing *wee-1.3(RNAi)* gonads and

512   mainly seen in *wee-1.3(RNAi)* animals with highly abnormal oocytes. GFP::LIN-41 is also

513   degraded prematurely after *wee-1.3(RNAi)*, but this can be seen in gonads with relatively normal

514   oocytes (Spike *et al.* 2014a), suggesting that LIN-41 might be more sensitive to CDK-1 activity.

515   We tested this idea by treating animals that co-express mSCARLET::LIN-41 and PUF-11::GFP

516   with *wee-1.3(RNAi)* and selectively examining gonads with large, well-organized oocytes. In

517   these animals, mSCARLET::LIN-41 was down-regulated in younger (more distal) oocytes

518   (Figure 4I) and, as a consequence, prematurely eliminated from oocytes more frequently than

519   PUF-11::GFP (in 11/12 instead of 6/12 gonads, respectively). Collectively, these results indicate

520   that active CDK-1 promotes the elimination of PUF-3 and PUF-11 and suggest that LIN-41

521   might be more sensitive to the dysregulatory effects of *wee-1.3(RNAi)*.

522   ### SCF$_{SEL-10}$ and APC ubiquitin ligases do not target PUF-3 for degradation

523   PUF-3 and PUF-11 are components of LIN-41 RNPs and appear to be eliminated in response to

524   the same signal and at a similar time as LIN-41. These observations suggested that PUF-3 and

525   PUF-11 might be degraded as a consequence of LIN-41 degradation. We therefore asked

526   whether they are targeted for elimination by the same SCF E3 ubiquitin ligase. LIN-41 persists in

527   early embryos after the RNAi-mediated knockdown of the highly similar Skp-related genes *skr-1*

528   and *skr-2,* the Cullin *cul-1*, the F-box substrate recognition subunit *sel-10* and in the *sel-10(lf)*

529   mutants *sel-10(ok1632)* and *sel-10(ar41)* (Spike *et al*. 2018). However PUF-3::GFP and PUF-

530   11::GFP are eliminated normally from the embryos of *lon-3(e2175) sel-10(ar41)* mutant animals

531   (Figure 4, C, D, G, and H) and after *skr-1/2(RNAi)* (n>30 animals for each PUF::GFP fusion

532   protein) and *cul-1(RNAi)* (n≥10 animals for each PUF::GFP fusion protein). A distinct, SEL-10-

533   independent mechanism must therefore promote the elimination of PUF-3 and PUF-11 from

534   early embryos. We conclude that the degradation of PUF-3 and PUF-11 during the OET is not a

535   consequence of the SEL-10-dependent degradation of LIN-41, consistent with the idea that

536   multiple mechanisms remodel and take apart oocyte RNPs during the OET.

537   An interesting feature of LIN-41 degradation is that it occurs even when the metaphase-

538   to-anaphase transition of the first meiotic division is blocked by disrupting the function of the

539   anaphase-promoting complex (APC) (Spike *et al.* 2014a). This feature distinguishes LIN-41

540   from proteins such as IFY-1/Securin (Kitagawa *et al.* 2002; Wang *et al.* 2013) and CYB-

541   1/Cyclin B1 (Liu *et al.* 2004), which are degraded slightly later than LIN-41 in an APC-

542   dependent fashion. Therefore, we tested whether the metaphase-to-anaphase transition regulates

543   the elimination of PUF-3::GFP by impairing the function of two key members of the APC, *mat-*

544   *1*/Apc3 and *emb-30*/Apc4 (Furuta *et al.* 2000; Shakes *et al.* 2003). *mat-1(RNAi)* caused fully

545   penetrant 1-cell embryonic arrest, but did not delay or prevent the elimination of PUF-3::GFP

546   from embryos (n = 25 animals). Likewise, PUF-3::GFP disappears normally from the embryos of

547   *emb-30(tn377*ts*)* mutants shifted to 25 °C at the L4 stage (n > 25); these embryos arrest in

548   metaphase during the first meiotic division (Furuta *et al.* 2000). PUF-11::GFP protein was not

549   tested using these assays. We conclude that, as for LIN-41, the elimination of PUF-3 from early

550   embryos does not require the activity of the APC. However, unlike LIN-41, the elimination of

551   PUF-3::GFP and PUF-11::GFP from embryos is *sel-10* independent.

552   ***Proteolysis and translational repression limit the expression of RNA-binding proteins during***
553   ***the OET***

554   Many of the oocyte-expressed proteins degraded during the OET in *C. elegans* are RNA-binding

555   proteins that regulate translation (reviewed by Robertson and Lin 2013, 2015). These RNA-

556   binding proteins include LIN-41 and the Pumilio/FBF-family RNA-binding proteins PUF-3 and

557   PUF-11. PUF-3 and PUF-11 function redundantly, repress the translation of specific targets in

558   oocytes, and play important roles in germline stem cells and embryonic development in *C.*

559   *elegans* (Hubstenberger *et al.* 2012; Haupt *et al.* 2020). Since PUF-3 and PUF-11 appear to be

560   degraded soon after meiotic maturation (Figure 3), it seems likely that the maternal-effect

27

561   embryonic lethality caused by an absence of both proteins is due to mRNA translation defects in

562   developing oocytes. Interestingly, the timing and regulation of PUF-3 and PUF-11 degradation

563   appear to be temporally and molecularly coordinated with meiotic maturation and strongly

564   resemble what we have described for LIN-41 (Spike *et al.* 2018 and Figure 3). The resemblances

565   include a requirement for active CDK-1 (Figure 4), which is essential for entry into meiotic M-

566   phase (Boxem *et al.* 1999, Burrows *et al.* 2006), and independence from APC ubiquitin ligase

567   subunits that promote the subsequent metaphase-to-anaphase transition (Furuta *et al.* 2000;

568   Shakes *et al.* 2003). Additional connections between LIN-41, PUF-3, and PUF-11 include the

569   identification of each protein and mRNA in purified LIN-41 RNPs, and the identification of

570   LIN-41 and PUF-3/11 as factors important for the 3'UTR-mediated translational repression of a

571   common target, the Rbfox-related RNA-binding protein SPN-4 (Hubstenberger *et al.* 2012;

572   Tsukamoto *et al*. 2017). These disparate observations suggest that LIN-41, PUF-3, and PUF-11

573   might collaborate and function, at least in part, as components of a regulatory RNP to inhibit the

574   translation of SPN-4 in developing oocytes. Previously, we proposed that LIN-41 is inactivated

575   as a translational repressor prior to its degradation (Spike *et al*. 2018). Since *cdk-1(RNAi)* does

576   not reduce or eliminate SPN-4::GFP expression in early embryos (Tsukamoto *et al.* 2017), we

577   suggest that PUF-3 and PUF-11 are likewise inactivated prior to their degradation. Thus, we

578   suggest that the activity of a LIN-41/PUF-3/PUF-11 RNP is down-regulated in a CDK-1-

579   independent manner near the end of oogenesis. This model is consistent with the observation that

580   SPN-4::GFP expression in embryos is scarcely affected when LIN-41 degradation is inhibited

581   (Spike *et al.* 2018). A detailed understanding of the SEL-10-independent mechanism underlying

582   the degradation of PUF-11 and PUF-3 would enable tests of this model.

583

584   *ETC-1/Hul5/UBE3C promotes efficient protein clearance during the OET*

585   Since PUF-3/11 are degraded in a SEL-10-independent manner, and because regulated protein

586   degradation often requires ubiquitination (reviewed by Dikic *et al.* 2017), we tested whether a

587   different ubiquitin ligase might promote the elimination of PUF-3::GFP from embryos. Many

588   potential ubiquitin ligases have been identified in *C. elegans*, including (1) multi-subunit E3s

589   (SCF-type, APC), (2) HECT-domain E3s, (3) U-box E3s, and (4) more than 100 RING-finger

590   proteins that might function as monomeric E3s (Kipreos *et al.* 2005). We performed a small-

591   scale RNAi screen that targeted the first three classes of ubiquitin ligases and identified the

592   HECT-domain ubiquitin ligase ETC-1/Hul5/UBE3C as a promising candidate. When animals

593   expressing both mSCARLET::LIN-41 and PUF-3::GFP [*lin-41(tn1892); puf-3(tn1820)*

594   genotype] were exposed to *etc-1(RNAi)*, there was no discernable change in mSCARLET::LIN-

595   41 degradation, yet elevated levels of GFP were observed in multiple young embryos (n=24/24

596   animals). This suggested that *etc-1* knock down specifically interferes with the elimination of

597   oocyte-expressed PUF-3::GFP but not mSCARLET::LIN-41. We confirmed these RNAi-based

598   observations with *etc-1(gk5182)*, a predicted loss-of-function allele, which introduces a

599   premature stop codon, generated by the *C. elegans* Reverse Genetics Core Facility at the

600   University of British Columbia (The *C. elegans* Deletion Mutant Consortium 2012). *etc-*

601   *1(gk5182); puf-3(tn1820)* and *etc-1(gk5182); puf-11(tn1824)* animals exhibit GFP fluorescence

602   in multiple embryos compared to *etc-1(+)* controls (Figure 5, A–D), while expanded

603   mSCARLET is not observed in *lin-41(tn1892); etc-1(gk5182)* animals (Figure 5, G and H).

604   ETC-1 was proposed to function as an E3 ubiquitin ligase that regulates the level of

605   cytoplasmic IFY-1/Securin and CYB-1/cyclin B1 in post-meiosis I embryos in *C. elegans* (Wang

606   *et al.* 2013). In that study, RNA interference was used to reduce *etc-1* function [*etc-1(RNAi)*] and

29

607   CYB-1 degradation was monitored using a transgene that uses heterologous regulatory elements

608   to drive the expression of a GFP::CYB-1 fusion protein in the *C. elegans* germline (*ekIs2[pie-*

609   *1p::gfp::cyb-1]*). We used a new viable and fertile allele of *cyb-1* that expresses a GFP-tagged

610   CYB-1 fusion protein (Figure S1C; CYB-1::GFP$_F$) to examine CYB-1::GFP expression in wild-

611   type and in *etc-1(gk5182)* embryos (Figure 5, E and F). Since CYB-1 is essential for viability

612   (van der Voet *et al.* 2009), the CYB-1::GFP fusion protein made by *cyb-1(tn1806[cyb-*

613   *1::gfp::3xflag])* homozygotes must be substantially functional *in vivo*. In otherwise wild-type

614   animals, CYB-1::GFP is reduced in young mitotic embryos relative to meiotic embryos and

615   oocytes (Figure 5E). However, in *etc-1(gk5182); cyb-1(tn1806)* embryos GFP levels continue to

616   remain high after meiosis (Figure 5F). We also confirmed that *etc-1(gk5182)* affects the

617   degradation of IFY-1::GFP (IFY-1::GFP$_F$) using the fosmid-based transgene *ddIs128[ify-*

618   *1::gfp::3xflag]* (Sarov *et al.* 2012). *etc-1(gk5182)* appears to have a relatively weak effect on

619   IFY-1::GFP (Figure 5, I and J) compared to PUF-3::GFP, PUF-11::GFP and CYB-1::GFP

620   (Figure 5, A–F). The amount of GFP fluorescence in post-meiotic *etc-1(gk5182); ddIs128*

621   embryos is only slightly elevated relative to *etc-1(+)* control embryos (Figure 5, I and J).

622

ETC-1 is broadly expressed and present in oocytes and early embryos

624   ETC-1 and its orthologs, Hul5 (yeast) and UBE3C (humans) have two well-defined structural

625   domains: an IQ domain close to the N-terminus and a HECT domain at the extreme C-terminus

626   (Figure 6A; Wang *et al.* 2013; Marín 2018). The HECT domain of UBE3C and other HECT-

627   domain E3 ubiquitin ligases has a well-defined function; it is essential for mediating the

628   acceptance and transfer of ubiquitin from an E2-conjugating enzyme to a degradation substrate

629   via a cysteine residue at its catalytic site (You and Pickart 2001; Singh and Sivaraman 2020;

630   reviewed in Lorenz 2018). The IQ domain-containing N-terminus of UBE3C mediates an

631   interaction with the proteasome that is also important for function, but this portion of UBE3C is

632   less well-conserved than the HECT domain and its function is less well-defined (You and Pickart

633   2001; You *et al.* 2003; Wang *et al*. 2013). Given this structural and functional information, we

634   decided to tag the extreme N-terminus with GFP to examine where ETC-1 is expressed and

635   localized in *C. elegans*.

636   When we examined the sequences at the 5' end of the *etc-1* gene (Figure 6A) it became

637   apparent that ETC-1 translation might begin 60 bp upstream of the annotated start codon (ATG

638   #2 in Figure 6A) (http://www.wormbase.org, release WS278). *etc-1* is the downstream gene in a

639   two gene operon and contains an annotated and sequence-verified trans-splice acceptor site

640   immediately adjacent to a possible start codon (ATG #1 in Figure 6A). In *C. elegans*, trans-

641   splicing is used to physically separate the co-transcribed messenger RNAs of an operon (Spieth

642   *et al.* 1993). We predicted that ETC-1 translation should be initiated at ATG #1 for the following

643   reasons: (1) start codons are commonly found within 10 bp of a trans-splice acceptor site (Allen

644   *et al*. 2011), and (2) after trans-splicing, ATG #1 would be the first start codon in the *etc-1*

645   mRNA. If correct, 20 additional amino acids would be appended to the N-terminus of the

646   predicted ETC-1 protein. Seven of these amino acids are similar or identical to equivalent

647   residues at the N-terminus of UBE3C (Figure 6B). We created two different GFP-tagged alleles

648   of *etc-1*: (1) *etc-1(tn1919[gfp::3xflag::etc-1#1])*, which places GFP (and another start codon)

649   immediately upstream of the start codon adjacent to the trans-splice acceptor site (ATG #1), and

650   (2) *etc-1(tn1920[gfp::3xflag::etc-1#2])*, which places an identical tag immediately upstream of

651   the annotated start codon (ATG #2) (Figure S4A). Both *etc-1(tn1919)* and *etc-1(tn1920)* express

652 GFP (Figure 6, C and D, and Figure S4, B and C) and make large fusion proteins that

653 approximate the predicted sizes of the GFP::ETC-1 fusion proteins (~150 kDa, see below)

654 (Figure 6E). We conclude that a start codon immediately adjacent to the *etc-1* 5' trans-splice site

655 is capable of initiating translation *in vivo*.

656 *etc-1(tn1919)* and *etc-1(tn1920)* express GFP::ETC-1 (labeled GFP$_F$::ETC-1) in the

657 oogenic germline of hermaphrodites, where it is both cytoplasmic and nucleoplasmic (Figure 6,

658 C and D). We observed no significant difference in the amount of cytoplasmic GFP::ETC-1 in

659 the germlines of *etc-1(tn1919)* (n=11) and *etc-1(tn1920)* (n=8) adult hermaphrodites ($P>0.1$

660 using a Student's *t*-test). In addition, both alleles express GFP::ETC-1 in embryos (Figure 6, C

661 and D) and in a variety of somatic tissues, including the intestine, the spermatheca, and

662 unidentified cells near the pharynx (arrow in Figure S4, B and C). Interestingly, *etc-1(tn1920)*

663 adult hermaphrodites (n=3) express 2.4-fold more GFP::ETC-1 in the unidentified cells near the

664 pharynx than *etc-1(tn1919)* adult hermaphrodites (n=7) ($P<1 \times 10^{-6}$ using a Student's *t*-test). This

665 result suggests there could be differential start codon usage in some cell types. In *etc-1(tn1920)*

666 animals, the start codon at the beginning of the GFP coding sequence is 60 bp downstream of

667 ATG #1 and in the same relative position as the annotated start codon (ATG #2) in the

668 endogenous *etc-1* gene (Figure S4A). We hypothesized that *etc-1(tn1920)* animals might be able

669 to initiate GFP::ETC-1 translation both at the start codon used by *etc-1(tn1919)* animals (150.5

670 kDa GFP::ETC-1) and at the start codon located at the beginning of the GFP coding sequence

671 (148 kDa GFP::ETC-1). Consistent with this idea, some of the GFP::ETC-1 made by *etc-*

672 *1(tn1920)* animals appears to migrate slightly faster on western blots (Figure 6E). These

673 observations suggest that ETC-1 translation can initiate at ATG #1 in most tissues, including the

674 germline, while leaving the possibility that ETC-1 translation also initiates at ATG #2 in some

675   somatic cells. However, it is also possible that the slightly different GFP expression patterns seen

676   in *etc-1(tn1919)* and *etc-1(tn1920)* are caused by a difference in gene structure that we have not

677   explicitly considered or the fact that these alleles are differently functional. As we will describe,

678   *etc-1(tn1919)* (ATG #1) appears to be largely functional during the OET, while *etc-1(tn1920)*

679   (ATG #2) resembles the strong loss-of-function *etc-1(gk5182)* allele.

680

681   ***ETC-1 may be non-essential, even when the function of the anaphase-promoting complex has***

682   ***been compromised***

683   *etc-1(RNAi)* and *etc-1(tm5615)* deletion animals are viable and fertile; they do not have an overt

684   phenotype in an otherwise wild-type background (Wang *et al.* 2013). *etc-1(gk5182)* animals are

685   also viable and fertile with no overt defects in oocyte or embryo development. Whereas *etc-*

686   *1(tm5615)* is predicted to be an in-frame deletion (Figure 6A), *etc-1(gk5182)* is a premature stop

687   codon in the second exon of the *etc-1* gene (Figure 6A) and should be a strong loss-of-function

688   allele. Because SEL-10 and ETC-1 both help degrade proteins during the first meiotic division,

689   we tested whether the strong loss-of-function mutation *sel-10(ar41)* (Figure S1A) would provide

690   a sensitized background to reveal defects. However, *etc-1(gk5182)*; *lon-3(e2175)* and *etc-*

691   *1(gk5182)*; *lon-3(e2175) sel-10(ar41)* hermaphrodites are essentially indistinguishable and

692   produce relatively large numbers of progeny (286 ± 26 larvae, n=14 parental animals, and 283 ±

693   29 larvae, n=15 parental animals, respectively, at 20 °C). These brood sizes are slightly reduced

694   relative to the wild type but essentially indistinguishable from the brood sizes of *lon-3(e2175)*

695   and *lon-3(e2175) sel-10(ar41)* hermaphrodites at 20 °C (Spike *et al.* 2018). Since Hul5, the

696   ETC-1 ortholog of budding yeast, facilitates the degradation of protein aggregates that form

33

697 during heat stress (Fang *et al*. 2011), we examined whether *etc-1(gk5182)* animals are unusually

698 sensitive to elevated temperatures. We failed to find any evidence that this is the case. *etc-*

699 *1(gk5182)* animals are homozygous viable and fertile at 25 °C and can be maintained at this

700 temperature for multiple generations. When wild-type animals are heat-stressed for 3 hours at 31

701 °C, partially penetrant embryonic lethality occurs in the 24-hour period immediately after the

702 stress is applied (Huelgas-Morales *et al.* 2016). Using this heat stress protocol, similar

703 percentages of embryos produced within the relevant 24-hour period died when we compared

704 animals with the *etc-1(gk5182)* genotype (21% lethality, n=565 embryos, n=12 animals) to the

705 wild type (26%, n=463 embryos, n=11 animals). Wild-type L4-stage larvae shifted from 20 °C to

706 37 °C for 1.5 hours exhibit partially penetrant larval arrest and lethality (Zevian and Yanowitz

707 2014). Using this protocol, similar percentages of wild-type (54%, n=268) and *etc-1(gk5182)*

708 mutant animals (48%, n=300) died after heat shock.

709 Wang *et al.* (2013) reported that *etc-1(RNAi)* strongly enhances the lethality of *mat-*

710 *1(ax161*ts*); him-8(e1489)* animals at 15 °C. This enhancement was used to support the idea that

711 ETC-1 and the anaphase promoting complex (APC) share redundant functions, including the

712 degradation of the key cell cycle regulators IFY-1/securin and CYB-1/Cyclin B. We revisited

713 this genetic interaction using *etc-1(gk5182)* and two different temperature-sensitive alleles that

714 attenuate APC function in *C. elegans*: *emb-30(tn377*ts*)* and *mat-1(ax161*ts*)* (Furuta *et al.* 2000,

715 Shakes *et al.* 2003). Contrary to expectation, we found that *etc-1(gk5182); emb-30(tn377*ts*)* and

716 *mat-1(ax161*ts*); etc-1(gk5182)* double mutants are each homozygous viable and fertile at 15 °C.

717 Since *mat-1(ax161*ts*)* was also used by Wang *et al.* (2013), we examined the number of larvae

718 produced by *mat-1(ax161*ts*); etc-1(gk5182)* and *mat-1(ax161*ts*)* parents. These animals were

719 initially derived from *mat-1*-balanced strains (Table S1). For each strain, we counted the number

34

720   of larvae produced by parents that were third-generation *mat-1(ax161*ts*)* homozygotes raised at

721   15 °C. *mat-1(ax161*ts*); etc-1(gk5182)* animals produced fewer progeny (100 ± 35 larvae, n=15

722   animals) than *mat-1(ax161*ts*)* animals (165 ± 46 larvae, n=17 animals) and this difference is

723   statistically significant (*P*=0.0001). However, the *mat-1(ax161*ts*); etc-1(gk5182)* double mutant

724   phenotype is not as severe as the phenotype described for *mat-1(ax161*ts*); him-8(e1489)*; *etc-*

725   *1(RNAi)* animals at 15 °C (Wang *et al.* 2013) and is not comparable to the phenotype of *mat-*

726   *1(ax161*ts*)* or *mat-1(ax161*ts*); him-8(e1489)* animals at 25 °C (Shakes *et al.* 2003).

727

GFP-fusion proteins are partially proteolyzed in etc-1(gk5182) animals

729   The PUF-3::GFP, PUF-11::GFP, CYB-1::GFP and IFY-1::GFP fusion proteins each contain

730   three FLAG epitope tags in addition to the fluorescent protein tag (Figure S1C, Sarov *et al.*

731   2012). We used an antibody that recognizes the FLAG tag to examine each fusion protein by

732   western blot in wild-type and *etc-1(gk5182)* hermaphrodites. Full-length PUF-3::GFP, PUF-

733   11::GFP and CYB-1::GFP migrate as expected in lysates made from both wild-type and *etc-*

734   *1(gk5182)* hermaphrodites (Figure 7A), while the IFY-1::GFP fusion protein migrates slightly

735   slower than expected (Figure 7D). However, in each *etc-1(gk5182)* lysate, a second band is also

736   recognized by the anti-FLAG antibody (Figure 7, A and D). This *etc-1(gk5182)*-specific band

737   only accumulates when a GFP fusion protein is present (Figure S5A) and can be recognized by a

738   GFP-specific antibody (Figure S5B). Depending on the GFP fusion protein, it migrates slightly

739   faster (Figure 7A) or slower (Figure 7D) than a 40 kDa molecular weight marker. But in each

740   case, the *etc-1(gk5182)*-specific band is predicted, based on size, to encompass the entire 31–32

741   kDa GFP::FLAG tag (File S2). We estimate that these GFP::FLAG fragments account for 10–

742   20% of the total signal in each *etc-1(gk5182); puf-3(tn1820[puf-3::gfp::3xflag])* lane, 4–11% of

743   the total signal in each *etc-1(gk5182); puf-11(tn1824[puf-11::gfp::3xflag)* lane and 4–10% of the

744   total signal in each *etc-1(gk5182); cyb-1(tn1806[cyb-1::gfp::3xflag])* lane (Figure 7).

745   GFP::FLAG fragments appear to be less abundant in *etc-1(gk5182); ddIs128[ify-1::gfp::3xflag]*

746   animals relative to the full length IFY-1::GFP fusion protein (Figure 7D), but we could not make

747   an accurate assessment of this difference because the full-length fusion protein and fragment

748   were not in the linear range of detection at the same time. These observations suggest that the

749   GFP fluorescence observed in *etc-1(gk5182)* embryos (Figure 5, A–F and I–J) may derive from

750   GFP::FLAG fragments rather than full-length PUF-3::GFP, PUF-11::GFP, CYB-1::GFP, or IFY-

751   1::GFP fusion proteins.

752   Our observations of GFP fluorescence in living *etc-1(lf)* animals suggest that *etc-*

753   *1(gk5182)* perturbs protein degradation during the OET (Figure 5). However, if the GFP::FLAG

754   fragments generated from each fusion protein accumulate prior to this time (during oogenesis,

755   for example), they might simply become easier to visualize when the full-length fusion protein is

756   degraded during the OET. We examined whether GFP::FLAG fragments are generated from the

757   PUF-3::GFP, PUF-11::GFP and CYB-1::GFP fusion proteins in unmated *etc-1(gk5182); fog-*

758   *2(oz40)* females to address this possibility. Development of the oogenic germline is normal in

759   *fog-2* mutant females, but due to the absence of the major sperm protein signal from sperm

760   (McCarter *et al.* 1999; Miller *et al.* 2001), the rate of oocyte meiotic maturation is substantially

761   decreased, and fertilization and embryo formation are prevented. We found that GFP::FLAG

762   fragments are generated from each fusion protein in *etc-1(gk5182); fog-2* females (Figure 7B;

763   see Figure S5D for a longer exposure). Relative to the amount of each full-length fusion protein,

764   however, GFP::FLAG fragments appear to be considerably less abundant in unmated *etc-*

36

765   *1(gk5182); fog-2* females than in *etc-1(gk5182)* hermaphrodites (compare Figure 7, A and B) or

766   mated *etc-1(gk5182); fog-2* females (compare Figure 7B and Figure S5, C and D). This was most

767   noticeable for the GFP::FLAG fragments derived from CYB-1::GFP and PUF-11::GFP. These

768   observations suggest that many of the GFP::FLAG fragments produced by *etc-1(gk5182)* mutant

769   hermaphrodites and mated females are generated when each GFP fusion protein is degraded

770   during the OET.

771   GFP::FLAG fragments also accumulate in *etc-1(gk5182); cyb-1(tn1806); fog-2(oz40)*

772   adult males (Figure 7B). Endogenous CYB-1 is abundant in the male germline and eliminated

773   toward the end of meiosis (Yoon *et al.* 2017). CYB-1::GFP exhibits a similar pattern of

774   accumulation in *fog-2* males (Figure S6, A and B). In *etc-1(gk5182); fog-2* males, however, a

775   GFP signal perdures past the stage where CYB-1::GFP is normally eliminated (Figure S6, C and

776   D). Much of this signal localizes to residual bodies (Figure S6, E and F). Residual bodies form at

777   the end of the second meiotic division and receive cellular materials that are not required during

778   subsequent stages of spermatogenesis (Ward *et al.* 1981; reviewed in Chu and Shakes 2013). It

779   seems likely that, as in *etc-1(gk5182)* embryos, the GFP fluorescence seen in *etc-1(gk5182)*

780   residual bodies derives from GFP::FLAG fragments that are formed when CYB-1::GFP is

781   degraded during meiosis.

782

783   ***ETC-1 may promote proteasome processivity***

784   Hul5 and UBE3C, the yeast and human orthologs of ETC-1, are proteasome-associated ubiquitin

785   ligases that help the proteasome degrade difficult substrates (Crosas *et al.* 2006; Fang *et al.* 2011;

786   Kuo and Goldberg 2017; Gottlieb *et al.* 2019). In this context, Hul5 and UBE3C are thought to

787   be important for the processive degradation of proteins that are stalled on the proteasome. This

788   hypothesis was based, in part, on experiments with GFP fusion proteins. In the absence of Hul5,

789   or after UBE3C knockdown, the proteasomal degradation of substrates consisting of an unstable

790   domain fused with the much more stable GFP domain is incomplete. This results in the

791   accumulation of stable GFP-containing fragments of the original fusion protein (Aviram and

792   Kornitzer 2010; Martinez-Noël *et al.* 2012; Chu *et al.* 2013). The experiments described in the

793   previous section strongly suggest that ETC-1 plays a similar role in *C. elegans*. We added to

794   these observations by examining additional GFP and non-GFP-tagged fusion proteins in *etc-1(lf)*

795   hermaphrodites, as described below.

796   ***GFP::ETC-1 fusion proteins:*** Neither GFP::ETC-1 fusion protein is partially processed to a

797   substantial extent (Figure 6E). To determine whether either GFP-tagged allele is functional *in*

798   *vivo*, we examined whether PUF-3::GFP is partially processed in *etc-1(tn1919)* and *etc-*

799   *1(tn1920)* hermaphrodites. GFP::FLAG fragments accumulate in PUF-3::GFP-expressing *etc-*

800   *1(tn1920)* animals and are similar in abundance to the GFP::FLAG fragments seen in *etc-*

801   *1(gk5182)* animals (Figure 6E). *etc-1(tn1920)* therefore appears to be a strong loss-of-function

802   mutation. Only a very small amount of the PUF-3::GFP-derived GFP::FLAG fragment

803   accumulates in *etc-1(tn1919)* animals (Figure 6E, see the longer exposure), suggesting that *etc-*

804   *1(tn1919)* retains a significant amount of function in the *C. elegans* germline. It is not clear why

805   GFP::ETC-1-derived GFP::FLAG fragments do not substantially accumulate in *etc-1(tn1920)*

806   animals. Possibly ETC-1 itself is not a substrate for proteasomal degradation. Alternatively, it is

807   possible that these fragments accumulate to a level that is below our detection threshold. In this

808   regard, it is worth noting that GFP::ETC-1 is expressed at much lower levels than PUF-3::GFP

809   (Figure 6E).

810   ***RNP-8::GFP fusion proteins:*** We created a GFP-tagged allele of *rnp-8* (Figure S1C; RNP-

811   8::GFP$_F$ in all figures) and found that RNP-8::GFP is abundantly expressed in oocytes and early

812   embryos (Figure S7A). We do not know whether this GFP-tagged allele of *rnp-8* (*rnp-*

813   *8(tn1860[rnp-8::gfp:3xflag])*) is functional *in vivo*. Although RNP-8 is thought to be degraded in

814   response to oocyte maturation (Kim *et al.* 2010), RNP-8::GFP is not strongly down-regulated

815   during the oocyte-to-embryo transition (Figure S7A). GFP fluorescence is not obviously

816   increased in *rnp-8(tn1860)*; *etc-1(gk5182)* animals compared to *etc-1(+)* control animals (Figure

817   S7, A and B). Nevertheless, a small proportion of the RNP-8::GFP fusion protein made by *rnp-*

818   *8(tn1860)* is partially processed into GFP::FLAG fragments in *etc-1(gk5182)* hermaphrodites

819   (Figure S5C).

820   ***LIN-41 fusion proteins:*** Only full-length mSCARLET::LIN-41 fusion proteins accumulate to a

821   substantial level in wild-type, *etc-1(gk5182)* and *sel-10(lf)* hermaphrodites (Figure 7C). We did

822   not detect mSCARLET::FLAG or DENDRA::FLAG fragments at elevated levels in *etc-*

823   *1(gk5182)*, *sel-10(ar41)* or *sel-10(ok1632)* animals (Figure 7C; Figure S5E). This is consistent

824   with the observation that the levels of fluorescence appear to be the same in embryos made by

825   wild-type and *etc-1(gk5182)* animals that express mSCARLET::LIN-41 (Figure 5, G and H) and

826   the conclusion that the *etc-1(gk5182)* mutation does not perturb the SEL-10-mediated

827   degradation of mSCARLET::LIN-41 or DENDRA::LIN-41 that we documented using

828   fluorescence microscopy (Figure 1, A and B; Figure 2). We tested whether GFP::LIN-41 would

829   behave in the same way by crossing our original GFP-tagged *lin-41(tn1541)* allele (Figure S1B;

830   GFP$_S$::LIN-41 below and in all figures) into an *etc-1(gk5182)* genetic background. However, we

831   found that GFP is not appropriately down-regulated in the embryos of *lin-41(tn1541)*; *etc-*

832   *1(gk5182)* hermaphrodites compared to *lin-41(tn1541)*; *etc-1(+)* controls (Figure S7, C and D).

833   These observations suggest that GFP$_S$::LIN-41 is partially processed in *etc-1(gk5182)*

834   hermaphrodites and imply that GFP-tagged fusion proteins might be more recalcitrant than other

835   fusion proteins to processivity-challenged proteasomes.

836   To rigorously investigate these possibilities, we created new *lin-41* alleles that express a

837   GFP::FLAG-tagged LIN-41 fusion protein (GFP$_F$::LIN-41). We isolated two independent

838   insertions that were given different allele names [*lin-41(tn2054[gfp::3xflag::lin-41])* and *lin-*

839   *41(tn2055[gfp::3xflag::lin-41])*, see Figure S1B]; these two alleles are molecularly identical and

840   were used interchangeably in our experiments. Interestingly, GFP fluorescence in GFP$_F$::LIN-41-

841   expressing worms is much brighter than in GFP$_S$::LIN-41-expressing worms (compare Figures

842   S7, E and G), possibly because the mRNA sequence that encodes the GFP::3xFLAG tag has a

843   much higher codon adaptation index (CAI=0.92) than the sequence that encodes the GFP::S tag

844   (CAI=0.28) (Redemann *et al*. 2011). More than half of the GFP$_F$::LIN-41-expressing animals

845   also exhibit a defect in egg laying (Egl phenotype) as adult hermaphrodites at 20°C (Figure

846   S7H). A similar phenotype is observed when LIN-41 is over-expressed in somatic cells during

847   the fourth larval (L4) stage by interfering with *let-7* microRNA regulation (e.g., using the *lin-*

848   *41(xe11*gf*)* allele described by Ecsedi *et al.* 2015). With respect to our tagged alleles of *lin-41*,

849   however, this defect uniquely characterizes the GFP::FLAG tagged alleles, as most GFP$_S$::LIN-

850   41 (Figure S7F), mSCARLET::LIN-41, and DENDRA::LIN-41-expressing adults do not have an

851   Egl phenotype. Despite these intriguing differences, the temporal expression pattern and

852   regulation of GFP$_F$::LIN-41 strongly resembles GFP$_S$::LIN-41. Most importantly, GFP$_F$::LIN-41-

853   expressing animals exhibit higher levels of GFP fluorescence in the early embryos made by *sel-*

854   *10(ok1632)* and *etc-1(gk5182)* mutants relative to otherwise wild-type hermaphrodites (Figure 5,

855   K and L; Figure S7, I–N). Interestingly, the subcellular localization pattern of GFP$_F$::LIN-41-

40

856   derived GFP fluorescence is distinctly different in the early embryos made by *sel-10(ok1632)*

857   and *etc-1(gk5182)* mutant hermaphrodites (Figure S7, K and M). In *sel-10(ok1632)* embryos,

858   GFP fluorescence is primarily cytoplasmic and appears to be enriched in ribonucleoprotein

859   particles called P granules (Figure S7M). Localization to embryonic P granules is also observed

860   when LIN-41 degron sequences are disrupted in GFP$_S$::LIN-41 (Spike *et al.* 2018). In *etc-*

861   *1(gk5182)* embryos, however, GFP fluorescence does not localize to P granules and is slightly

862   enriched in the nucleus (Figure S7K). These observations are consistent with the idea that

863   GFP$_F$::LIN-41 is partially processed into a GFP-containing protein fragment that is largely

864   responsible for the excess fluorescence observed in early *etc-1(gk5182)* embryos.

865   The only difference between GFP$_F$:::LIN-41, mSCARLET::LIN-41 and DENDRA::LIN-

866   41 is the fluorescent protein fused to LIN-41 (Figure S1B). We examined all of these proteins in

867   *etc-1(gk5182)* and *etc-1(+)* hermaphrodites by western blot, and confirmed that GFP::FLAG

868   fragments accumulate in GFP$_F$:::LIN-41-expressing *etc-1(gk5182)* adults at elevated levels

869   relative to *etc-1(+)* animals (Figure 7E). A longer exposure of the same western blot revealed

870   low levels of GFP::FLAG fragments even in *etc-1(+)* hermaphrodites (Figure S5F). However,

871   *etc-1*-dependent fragments derived from the mSCARLET::LIN-41 and DENDRA::LIN-41

872   fusion proteins were not observed. We conclude that *etc-1(gk5182)* specifically disrupts the

873   proteolysis of the GFP-containing LIN-41 fusion proteins (GFP$_F$::LIN-41 and GFP$_S$::LIN-41)

874   and speculate that tagging LIN-41 with GFP creates a LIN-41 fusion protein that is more

875   difficult to degrade. Consistent with this idea, GFP is known to be a particularly stable

876   fluorescent protein that can be difficult for the proteasome to degrade (Khmelinskii *et al.* 2016;

877   Reichard *et al.* 2016; Bragança and Kraut 2020). Based on these observations, we propose that

878   fusion with GFP is an important cause of the proteolysis defects observed in *etc-1(gk5182)*

879   animals (Figures 5 and 7). In this context, we note the study that identified and described ETC-1

880   as a target-specific E3 ubiquitin ligase in *C. elegans* (Wang *et al.* 2013) relied on GFP fusion

881   proteins and monitored protein degradation by looking exclusively at fluorescence. Our

882   observations suggest, instead, that the *C. elegans etc-1* gene has the same type of activity

883   described for orthologous genes in yeast and humans (Aviram and Kornitzer 2010; Martinez-

884   Noël *et al.* 2012; Chu *et al.* 2013) and that the ETC-1 protein promotes proteasome processivity,

885   which may be especially important during the OET when many proteins are targeted for efficient

886   proteasomal degradation.

ETC-1/Hul5/UBE3C, GFP fusion proteins, and proteasome processivity

888   Wang *et al.* (2013) identified and described ETC-1 (UB*E T*hree *C*), the *C. elegans* UBE3C

889   ortholog, as a HECT-type E3 ubiquitin ligase that promotes the degradation of the essential cell

890   cycle proteins IFY-1/Securin and CYB-1/Cyclin B1 during the OET. Degradation was monitored

891   using a GFP fusion protein (IFY-1::GFP or GFP::CYB-1), immunoprecipitation assays clearly

892   documented a specific interaction between the GFP fusion protein and ETC-1, and *in vitro*

893   assays confirmed that ETC-1 is able to interact with, and ubiquitylate, each target protein.

894   Although these findings were consistent with the interpretation that ETC-1 functions as an E3

895   ubiquitin ligase, they are also compatible with our results that suggest instead that ETC-1

896   functions as an E4 enzyme that mediates ubiquitin chain elongation for the processive

897   degradation of proteins already targeted for ubiquitin conjugation by E3 enzymes—a function

898   shown for Hul5 in budding yeast (Crosas *et al*. 2006). Thus, the observations of Wang *et al*.

899   (2013) at the time supported a simple and sensible model: that ETC-1 and the anaphase

900   promoting complex target the same *C. elegans* proteins (e.g., IFY-1 and CYB-1) for

901   ubiquitination and degradation. This model was also supported by the observation that *etc-*

42

902   *1(RNAi)* strongly enhances the phenotype of mutants with a compromised APC. As described in

903   a previous section, we revisited the latter idea using *etc-1(gk5182)*; although there was evidence

904   of a genetic interaction between *etc-1(gk5182)* and *mat-1(ax161*ts*)* that might indicate a role for

905   ETC-1 in protein degradation during the OET, we did not observe a strongly enhanced

906   phenotype.

907   ***Caveats for analyzing the in vivo dynamics of protein degradation using GFP-fusion proteins***

908   Our analyses of several different GFP fusion proteins, including GFP fusions with IFY-1 and

909   CYB-1, provide a significantly more complicated explanation for the apparent perdurance of

910   each protein in the absence of ETC-1. It appears that the addition of a GFP moiety to several

911   proteins that are rapidly degraded during the OET, such as IFY-1, CYB-1, PUF-3, PUF-11, or

912   LIN-41, creates fusion proteins that are incompletely degraded in the absence of *etc-1* function.

913   Incomplete degradation results in the accumulation of a partial GFP-containing fragment in

914   embryos that is easily confused for the full-length GFP fusion protein when only fluorescence is

915   examined. Evidence that the GFP moiety is a determining factor is derived from our analysis of

916   LIN-41 fusion proteins. LIN-41 fusion proteins containing one of three different fluorescent

917   proteins, mSCARLET, DENDRA or GFP, were examined and the only fusion protein that was

918   incompletely degraded in an ETC-1-dependent manner was GFP::LIN-41 (Figure 7E). Our

919   experiments do not demonstrate, however, that the fused portion of the *C. elegans* protein is not

920   important for determining whether substrate processivity is substantively reduced in the absence

921   of ETC-1. Indeed, the GFP::ETC-1 fusion protein made by the loss-of-function *etc-1(tn1920)*

922   may not be partially processed (Figure 6E). Although it is tempting to speculate that this is

923   because GFP::ETC-1 is not obviously unstable during the OET (Figure 6D), our experiments

924   with RNP-8::GFP (Figure S5C and S7B) and unmated females (Figure 7B) argue for a more

925   nuanced view. In the unmated females, for example, it seems likely the proteasome still helps to

926   degrade or "turn over" each GFP fusion protein, but the proteins are relatively stable and many

927   fewer fragments are formed in the absence of *etc-1* function. In fact, it would be surprising if the

928   *C. elegans* protein fused to GFP is of no importance whatsoever; sequences outside the GFP

929   moiety are important for the Hul5-dependent proteolytic processing of a GFP-Pcl5 fusion protein

930   in *S. cerevisiae* (Aviram and Kornitzer 2010), and it is becoming increasingly clear that the

931   method and type of substrate ubiquitination influences proteasome processivity (Reichard *et al*.

932   2016; Bragança and Kraut 2020). Taken together, we believe our experiments with ETC-1

933   update the literature to show that ETC-1 plays a conserved role to promote proteasome

934   processivity and provide a cautionary note on the need to analyze endogenous proteins where

935   possible, utilize multiple protein tags and, ideally, analyze proteins on western blots when

936   studying protein degradation *in vivo*. Fortunately, the ease and rapidity of genome editing

937   continues to revolutionize the ability to conduct such experiments in the *C. elegans* system

938   (reviewed by Nance and Frøkjaer-Jensen 2019).

ACKNOWLEDGMENTS

946

LITERATURE CITED

Allen, A. K., J. E. Nesmith, and A. Golden, 2014 An RNAi-based suppressor screen identifies interactors of the Myt1 ortholog of *Caenorhabditis elegans*. G3 (Bethesda) 4: 2329–2343.

Allen, M. A., L. W. Hillier, R. H. Waterston, and T. Blumenthal, 2011 A global analysis of *C. elegans* trans-splicing. Genome Res 21: 255–264.

Arribere, J. A., R. T. Bell, B. X. Fu, K. L. Artiles, P. S. Hartman *et al.*, 2014 Efficient marker-free recovery of custom genetic modifications with CRISPR/Cas9 in *Caenorhabditis elegans*. Genetics 198: 837–846.

Aviram, S., and D. Kornitzer, 2010 The ubiquitin ligase Hul5 promotes proteasomal processivity. Mol Cell Biol 30: 985–994.

Bachvarova, R., E. H. Davidson, V. G. Allfrey, and A. E. Mirsky, 1966 Activation of RNA synthesis associated with gastrulation. Proc Natl Acad Sci U S A 55: 358–365.

Blitz, I. L., and K. W. Y. Cho, 2021 Control of zygotic genome activation in *Xenopus*. Curr Top Dev Biol 145: 167–204.

Boxem, M., D. G. Srinivasan, and S. van den Heuvel, 1999 The *Caenorhabditis elegans* gene *ncc-1* encodes a cdc2-related kinase required for M phase in meiotic and mitotic cell divisions, but not for S phase. Development 126: 2227–2239.

Bragança, C. E., and D. A. Kraut, 2020 Mode of targeting to the proteasome determines GFP fate. J Biol Chem 295: 15892–15901.

Burrows, A. E., B. K. Sceurman, M. E. Kosinski, C. T. Richie, P. L. Sadler *et al.*, 2006 The *C. elegans* Myt1 ortholog is required for the proper timing of oocyte maturation. Development 133: 697–709.

970   Cao, W. X., A. Karaiskakis, S. Lin, S. Angers, and H. D. Lipshitz, 2021 The F-box protein Bard

971   (CG14317) targets the Smaug RNA-binding protein for destruction during the

972   *Drosophila* maternal-to-zygotic transition. Genetics in press.

973   Cao, W. X., S. Kabelitz, M. Gupta, E. Yeung, S. Lin *et al.*, 2020 Precise temporal regulation of

974   post-transcriptional repressors is required for an orderly *Drosophila* maternal-to-zygotic

975   transition. Cell Rep 31: 107783.

976   Chang, H. M., N. J. Martinez, J. E. Thornton, J. P. Hagan, K. D. Nguyen *et al.*, 2012 Trim71

977   cooperates with microRNAs to repress Cdkn1a expression and promote embryonic stem

978   cell proliferation. Nat Commun 3: 923.

979   Chen, J., F. Lai, and L. Niswander, 2012 The ubiquitin ligase mLin41 temporally promotes

980   neural progenitor cell maintenance through FGF signaling. Genes Dev 26: 803–815.

981   Choi, W. J., M. W. Clark, J. X. Chen, and A. Y. Jong, 1990 The CDC4 gene product is

982   associated with the yeast nuclear skeleton. Biochem Biophys Res Commun 172: 1324–

983   1330.

984   Chu, B. W., K. M. Kovary, J. Guillaume, L. C. Chen, M. N. Teruel *et al.*, 2013 The E3 ubiquitin

985   ligase UBE3C enhances proteasome processivity by ubiquitinating partially proteolyzed

986   substrates. J Biol Chem 288: 34575–34587.

987   Chu, D. S., and D. C. Shakes, 2013 Spermatogenesis. Adv Exp Med Biol 757: 171–203.

988   Chudakov, D. M., S. Lukyanov, and K. A. Lukyanov, 2007 Using photoactivatable fluorescent

989   protein Dendra2 to track protein movement. Biotechniques 42: 553–563.

990   Clegg, K. B., and L. Pikó, 1982 RNA synthesis and cytoplasmic polyadenylation in the one-cell

991   mouse embryo. Nature 295: 343–344.

992   Collins, G. A., and A. L. Goldberg, 2017 The logic of the 26S proteasome. Cell 169: 792–806.

993   Crosas, B., J. Hanna, D. S. Kirkpatrick, D. P. Zhang, Y. Tone *et al.*, 2006 Ubiquitin chains are

994   remodeled at the proteasome by opposing ubiquitin ligase and deubiquitinating activities.

995   Cell 127: 1401–1413.

996   Cuevas, E., A. Rybak-Wolf, A. M. Rohde, D. T. Nguyen, and F. G. Wulczyn, 2015

997   Lin41/Trim71 is essential for mouse development and specifically expressed in postnatal

998   ependymal cells of the brain. Front Cell Dev Biol 3: 20.

999   de la Cova, C. and I. Greenwald, 2012 SEL-10/Fbw7-dependent negative feedback regulation of

1000   LIN-45/Braf signaling in *C. elegans* via a conserved phosphodegron. Genes Dev 26:

1001   2524–2535.

1002 Dejima, K., S. Hori, S. Iwata, Y. Suehiro, S. Yoshina *et al.*, 2018 An aneuploidy-free and

1003   structurally defined balancer chromosome toolkit for *Caenorhabditis elegans*. Cell Rep

1004   22: 232–241.

1005 Deshaies, R. J., and J. E. Ferrell, 2001 Multisite phosphorylation and the countdown to S phase.

1006   Cell 107: 819–822.

1007 Dickinson, D. J., A. M. Pani, J. K. Heppert, C. D. Higgins, and B. Goldstein, 2015 Streamlined

1008   genome engineering with a self-excising drug selection cassette. Genetics 200: 1035–

1009   1049.

1010 Dikic, I., 2017 Proteasomal and autophagic degradation systems. Annu Rev Biochem 86: 193–

1011   224.

1012 Ding, M., D. Chao, G. Wang, and K. Shen, 2007 Spatial regulation of an E3 ubiquitin ligase

1013   directs selective synapse elimination. Science 317: 947–951.

1014 Dorfman, M., J. E. Gomes, S. O'Rourke, and B. Bowerman, 2009 Using RNA interference to

1015   identify specific modifiers of a temperature-sensitive, embryonic-lethal mutation in the

1016   *Caenorhabditis elegans* ubiquitin-like Nedd8 protein modification pathway E1-activating

1017   gene *rfl-1*. Genetics 182: 1035–1049.

1018   Ecsedi, M., M. Rausch, and H. Großhans, 2015 The *let-7* microRNA directs vulval development

1019   through a single target. Dev Cell 32: 335–344.

1020   Edgar, L. G., N. Wolf, and W. B. Wood, 1994 Early transcription in *Caenorhabditis elegans*

1021   embryos. Development 120: 443–451.

1022   Fang, N. N., A. H. Ng, V. Measday, and T. Mayor, 2011 Hul5 HECT ubiquitin ligase plays a

1023   major role in the ubiquitylation and turnover of cytosolic misfolded proteins. Nat Cell

1024   Biol 13: 1344–1352.

1025   Finley, D., 2009 Recognition and processing of ubiquitin-protein conjugates by the proteasome.

1026   Annu Rev Biochem 78: 477–513.

1027   Furey, C. G., J. Choi, S. C. Jin, X. Zeng, A. T. Timberlake *et al.*, 2018 De Novo mutation in

1028   genes regulating neural stem cell fate in human congenital hydrocephalus. Neuron 99:

1029   302–314.

1030   Furuta, T., S. Tuck, J. Kirchner, B. Koch, R. Auty *et al.*, 2000 EMB-30: an APC4 homologue

1031   required for metaphase-to-anaphase transitions during meiosis and mitosis in

1032   *Caenorhabditis elegans*. Mol Biol Cell 11: 1401–1419.

1033   Gallo, C. M., J. T. Wang, F. Motegi, and G. Seydoux, 2010 Cytoplasmic partitioning of P

1034   granule components is not required to specify the germline in *C. elegans*. Science 330:

1035   1685–1689.

1036   Gottlieb, C. D., A. C. S. Thompson, A. Ordureau, J. W. Harper, and R. R. Kopito, 2019 Acute

1037   unfolding of a single protein immediately stimulates recruitment of ubiquitin protein

1038   ligase E3C (UBE3C) to 26S proteasomes. J Biol Chem 294: 16511–16524.

1039   Govindan, J. A., H. Cheng, J. E. Harris, and D. Greenstein, 2006 $G\alpha_{o/i}$ and $G\alpha_s$ signaling

1040   function in parallel with the MSP/Eph receptor to control meiotic diapause in *C. elegans*.

1041   Curr Biol 16: 1257–1268.

1042   Green, R. A., A. Audhya, A. Pozniakovsky, A. Dammermann, H. Pemble *et al.*, 2008 Expression

1043   and imaging of fluorescent proteins in the *C. elegans* gonad and early embryo. Methods

1044   Cell Biol 85: 179–218.

1045   Griffin, E. E., D. J. Odde, and G. Seydoux, 2011 Regulation of the MEX-5 gradient by a

1046   spatially segregated kinase/phosphatase cycle. Cell 146: 955–968.

1047   Gurskaya, N. G., V. V. Verkhusha, A. S. Shcheglov, D. B. Staroverov, T. V. Chepurnykh *et al.*,

1048   2006 Engineering of a monomeric green-to-red photoactivatable fluorescent protein

1049   induced by blue light. Nat Biotechnol 24: 461–465.

1050   Hamatani, T., M. G. Carter, A. A. Sharov, and M. S. Ko, 2004 Dynamics of global gene

1051   expression changes during mouse preimplantation development. Dev Cell 6: 117–131.

1052   Harris, T. W., J. Baran, T. Bieri, A. Cabunoc, J. Chan *et al.*, 2014 WormBase 2014: new views

1053   of curated biology. Nucleic Acids Res. 42: D789–D793.

1054   Harrison, M. M., and M. B. Eisen, 2015 Transcriptional activation of the zygotic genome in

1055   *Drosophila*. Curr Top Dev Biol 113: 85–112.

1056   Haupt, K. A., K. T. Law, A. L. Enright, C. R. Kanzler, H. Shin *et al.*, 2020 A PUF hub drives

1057   self-renewal in *Caenorhabditis elegans* germline stem cells. Genetics 214: 147–161.

1058   Herrera, R. A., K. Kiontke, and D. H. Fitch, 2016 Makorin ortholog LEP-2 regulates LIN-28

1059   stability to promote the juvenile-to-adult transition in *Caenorhabditis elegans*.

1060   Development 143: 799–809.

1061   Hubbard, E. J., G. Wu, J. Kitajewski, and I. Greenwald, 1997 *sel-10*, a negative regulator of *lin-*

1062   *12* activity in *Caenorhabditis elegans*, encodes a member of the CDC4 family of

1063   proteins. Genes Dev 11: 3182–3193.

1064   Hubstenberger, A., C. Cameron, R. Shtofman, S. Gutman, and T. C. Evans, 2012 A network of

1065   PUF proteins and Ras signaling promote mRNA repression and oogenesis in *C. elegans*.

1066   Dev Biol 366: 218–231.

1067   Huelgas-Morales, G., and D. Greenstein, 2018 Control of oocyte meiotic maturation in *C.*

1068   *elegans*. Semin Cell Dev Biol 84: 90–99.

1069   Huelgas-Morales, G., C. G. Silva-García, L. S. Salinas, D. Greenstein, and R. E. Navarro, 2016

1070   The stress granule RNA-binding protein TIAR-1 protects female germ cells from heat

1071   shock in *Caenorhabditis elegans*. G3 (Bethesda) 6: 1031–1047.

1072   Jan, E., C. K. Motzny, L. E. Graves, and E. B. Goodwin, 1999 The STAR protein, GLD-1, is a

1073   translational regulator of sexual identity in *Caenorhabditis elegans*. EMBO J 18: 258–

1074   269.

1075   Jin, S. C., W. Dong, A. J. Kundishora, S. Panchagnula, A. Moreno-De-Luca *et al.*, 2020 Exome

1076   sequencing implicates genetic disruption of prenatal neuro-gliogenesis in sporadic

1077   congenital hydrocephalus. Nat Med 26: 1754–1765.

1078   Kanamoto, T., K. Terada, H. Yoshikawa, and T. Furukawa, 2006 Cloning and regulation of the

1079   vertebrate homologue of *lin-41* that functions as a heterochronic gene in *Caenorhabditis*

1080   *elegans*. Dev Dyn 235: 1142–1149.

1081   Kelly, W. G., S. Xu, M. K. Montgomery, and A. Fire, 1997 Distinct requirements for somatic

1082   and germline expression of a generally expressed *Caernorhabditis elegans* gene.

1083   Genetics 146: 227–238.

1084   Khmelinskii, A., M. Meurer, C. T. Ho, B. Besenbeck, J. Füller *et al.*, 2016 Incomplete

1085   proteasomal degradation of green fluorescent proteins in the context of tandem

1086   fluorescent protein timers. Mol Biol Cell 27: 360–370.

1087   Kim, K. W., T. L. Wilson, and J. Kimble, 2010 GLD-2/RNP-8 cytoplasmic poly(A) polymerase

1088   is a broad-spectrum regulator of the oogenesis program. Proc Natl Acad Sci U S A 107:

1089   17445–17450.

1090   Kipreos, E. T., 2005 Ubiquitin-mediated pathways in *C. elegans*. WormBook: 1–24.

1091   Kisielnicka, E., R. Minasaki, and C. R. Eckmann, 2018 MAPK signaling couples SCF-mediated

1092   degradation of translational regulators to oocyte meiotic progression. Proc Natl Acad Sci

1093   U S A 115: E2772–E2781.

1094   Kitagawa, R., E. Law, L. Tang, and A. M. Rose, 2002 The Cdc20 homolog, FZY-1, and its

1095   interacting protein, IFY-1, are required for proper chromosome segregation in

1096   *Caenorhabditis elegans*. Curr Biol 12: 2118–2123.

1097   Kloosterman, W. P., E. Wienholds, R. F. Ketting, and R. H. Plasterk, 2004 Substrate

1098   requirements for *let-7* function in the developing zebrafish embryo. Nucleic Acids Res

1099   32: 6284–6291.

1100   Kotani, T., K. Maehata, and N. Takei, 2017 Regulation of translationally repressed mRNAs in

1101   zebrafish and mouse oocytes. Results Probl Cell Differ 63: 297–324.

1102   Kuo, C. L., and A. L. Goldberg, 2017 Ubiquitinated proteins promote the association of

1103   proteasomes with the deubiquitinating enzyme Usp14 and the ubiquitin ligase Ube3c.

1104   Proc Natl Acad Sci U S A 114: E3404–E3413.

1105   Lambert, T. J., 2019 FPbase: a community-editable fluorescent protein database. Nat Methods

1106   16: 277–278.

1107   Latham, K. E., J. I. Garrels, C. Chang, and D. Solter, 1991 Quantitative analysis of protein

1108   synthesis in mouse embryos. I. Extensive reprogramming at the one- and two-cell stages.

1109   Development 112: 921–932.

1110 Lau, N. C., L. P. Lim, E. G. Weinstein, and D. P. Bartel, 2001 An abundant class of tiny RNAs

1111   with probable regulatory roles in *Caenorhabditis elegans*. Science 294: 858–862.

1112 Lin, Y. C., L. C. Hsieh, M. W. Kuo, J. Yu, H. H. Kuo *et al.*, 2007 Human TRIM71 and its

1113   nematode homologue are targets of *let-7* microRNA and its zebrafish orthologue is

1114   essential for development. Mol Biol Evol 24: 2525–2534.

1115 Liu, J., S. Vasudevan, and E. T. Kipreos, 2004 CUL-2 and ZYG-11 promote meiotic anaphase II

1116   and the proper placement of the anterior-posterior axis in *C. elegans*. Development 131:

1117   3513–3525.

1118 Liu, Q., X. Chen, M. K. Novak, S. Zhang, and W. Hu, 2021 Repressing Ago2 mRNA translation

1119   by Trim71 maintains pluripotency through inhibiting *let-7* microRNAs. Elife 10: e66288.

1120 Lorenz, S., 2018 Structural mechanisms of HECT-type ubiquitin ligases. Biol Chem 399: 127–

1121   145.

1122 Luong, X. G., and M. Conti, 2019 RNA binding protein networks and translational regulation in

1123   oocytes. In *Human Reproductive and Prenatal Genetics*, edited by P. C. K. Leung and J.

1124   Qiao. Academic Press, Cambridge.

1125 Maller Schulman, B. R., X. Liang, C. Stahlhut, C. DelConte, G. Stefani *et al.*, 2008 The *let-7*

1126   microRNA target gene, *Mlin41/Trim71* is required for mouse embryonic survival and

1127   neural tube closure. Cell Cycle 7: 3935–3942.

1128 Martínez-Noël, G., J. T. Galligan, M. E. Sowa, V. Arndt, T. M. Overton *et al.*, 2012

1129   Identification and proteomic analysis of distinct UBE3A/E6AP protein complexes. Mol

1130   Cell Biol 32: 3095–3106.

1131   Marín, I., 2018 Origin and evolution of fungal HECT ubiquitin ligases. Sci Rep 8: 6419.

1132   Matsuura, R., T. Ashikawa, Y. Nozaki, and D. Kitagawa, 2016 LIN-41 inactivation leads to

1133   delayed centrosome elimination and abnormal chromosome behavior during female

1134   meiosis in *Caenorhabditis elegans*. Mol Biol Cell 27: 799–811.

1135   McCarter, J., B. Bartlett, T. Dang, and T. Schedl, 1999 On the control of oocyte meiotic

1136   maturation and ovulation in *Caenorhabditis elegans*. Dev Biol 205: 111–128.

1137   McNally, K., A. Audhya, K. Oegema, and F. J. McNally, 2006 Katanin controls mitotic and

1138   meiotic spindle length. J Cell Biol 175: 881–891.

1139   Miller, M. A., V. Q. Nguyen, M.-H. Lee, M. Kosinski, T. Schedl *et al.*, 2001 A sperm

1140   cytoskeletal protein that signals oocyte meiotic maturation and ovulation. Science 291:

1141   2144–2147.

1142   Mitschka, S., T. Ulas, T. Goller, K. Schneider, A. Egert *et al.*, 2015 Co-existence of intact

1143   stemness and priming of neural differentiation programs in mES cells lacking Trim71.

1144   Sci Rep 5: 11126.

1145   Nance, J., and C. Frøkjær-Jensen, 2019 The *Caenorhabditis elegans* transgenic toolbox. Genetics

1146   212: 959–990.

1147   Newport, J., and M. Kirschner, 1982a A major developmental transition in early *Xenopus*

1148   embryos: I. Characterization and timing of cellular changes at the midblastula stage. Cell

1149   30: 675–686.

1150   Newport, J., and M. Kirschner, 1982b A major developmental transition in early *Xenopus*

1151   embryos: II. Control of the onset of transcription. Cell 30: 687–696.

1152   Nishi, Y., and R. Lin, 2005 DYRK2 and GSK-3 phosphorylate and promote the timely

1153   degradation of OMA-1, a key regulator of the oocyte-to-embryo transition in *C. elegans*.

1154   Dev Biol 288: 139–149.

1155   O'Farrell, F., S. S. Esfahani, Y. Engström, and P. Kylsten, 2008 Regulation of the *Drosophila*

1156   *lin-41* homologue *dappled* by *let-7* reveals conservation of a regulatory mechanism

1157   within the LIN-41 subclade. Dev Dyn 237: 196–208.

1158   Pritchard, D. K., and G. Schubiger, 1996 Activation of transcription in *Drosophila* embryos is a

1159   gradual process mediated by the nucleocytoplasmic ratio. Genes Dev 10: 1131–1142.

1160   Redemann, S., S. Schloissnig, S. Ernst, A. Pozniakowsky, S. Ayloo *et al.*, 2011 Codon

1161   adaptation-based control of protein expression in *C. elegans*. Nat Methods 8: 250–252.

1162   Reichard, E. L., G. G. Chirico, W. J. Dewey, N. D. Nassif, K. E. Bard *et al.*, 2016 Substrate

1163   ubiquitination controls the unfolding ability of the proteasome. J Biol Chem 291: 18547–

1164   18561.

1165   Reinhart, B. J., F. J. Slack, M. Basson, A. E. Pasquinelli, J. C. Bettinger *et al.*, 2000 The 21-

1166   nucleotide *let-7* RNA regulates developmental timing in *Caenorhabditis elegans*. Nature

1167   403: 901–906.

1168   Robertson, S., and R. Lin, 2013 The oocyte-to-embryo transition. Adv Exp Med Biol 757: 351–

1169   372.

1170   Robertson, S., and R. Lin, 2015 The maternal-to-zygotic transition in *C. elegans*. Curr Top Dev

1171   Biol 113: 1–42.

1172   Rose, K. L., V. P. Winfrey, L. H. Hoffman, D. H. Hall, T. Furuta *et al.*, 1997 The POU gene *ceh-*

1173   *18* promotes gonadal sheath cell differentiation and function required for meiotic

1174   maturation and ovulation in *Caenorhabditis elegans*. Dev Biol 192: 59–77.

1175   Rosu, S., and O. Cohen-Fix, 2017 Live-imaging analysis of germ cell proliferation in the *C.*

1176   *elegans* adult supports a stochastic model for stem cell proliferation. Dev Biol 423: 93–

1177   100.

1178   Rosu, S., and O. Cohen-Fix, 2020 Tracking germline stem cell dynamics *in vivo* in *C. elegans*

1179   using photoconversion. Methods Mol Biol 2150: 11–23.

1180   Rybak, A., H. Fuchs, K. Hadian, L. Smirnova, E. A. Wulczyn *et al.*, 2009 The *let-7* target gene

1181   mouse *lin-41* is a stem cell specific E3 ubiquitin ligase for the miRNA pathway protein

1182   Ago2. Nat Cell Biol 11: 1411–1420.

1183   Sarov, M., J. I. Murray, K. Schanze, A. Pozniakovski, W. Niu *et al.*, 2012 A genome-scale

1184   resource for *in vivo* tag-based protein function exploration in *C. elegans*. Cell 150: 855–

1185   866.

1186   Schneider, C. A., W. S. Rasband, and K. W. Eliceiri, 2012 NIH Image to ImageJ: 25 years of

1187   image analysis. Nat Methods 9: 671–675.

1188   Seydoux, G., and A. Fire, 1994 Soma-germline asymmetry in the distributions of embryonic

1189   RNAs in *Caenorhabditis elegans*. Development 120: 2823–2834.

1190   Sha, Q. Q., X. X. Dai, Y. Dang, F. Tang, J. Liu *et al.*, 2017 A MAPK cascade couples maternal

1191   mRNA translation and degradation to meiotic cell cycle progression in mouse oocytes.

1192   Development 144: 452–463.

1193   Shakes, D. C., P. L. Sadler, J. M. Schumacher, M. Abdolrasulnia, and A. Golden, 2003

1194   Developmental defects observed in hypomorphic anaphase-promoting complex mutants

1195   are linked to cell cycle abnormalities. Development 130: 1605–1620.

1196   Shirayama, M., M. C. Soto, T. Ishidate, S. Kim, K. Nakamura *et al.*, 2006 The conserved kinases

1197   CDK-1, GSK-3, KIN-19, and MBK-2 promote OMA-1 destruction to regulate the

1198   oocyte-to-embryo transition in *C. elegans*. Curr Biol 16: 47–55.

1199   Singh, S., and J. Sivaraman, 2020 Crystal structure of HECT domain of UBE3C E3 ligase and its

1200   ubiquitination activity. Biochem J 477: 905–923.

1201 Slack, F. J., M. Basson, Z. Liu, V. Ambros, H. R. Horvitz *et al.*, 2000 The *lin-41* RBCC gene

1202   acts in the *C. elegans* heterochronic pathway between the *let-7* regulatory RNA and the

1203   LIN-29 transcription factor. Mol Cell 5: 659–669.

1204 Spieth, J., G. Brooke, S. Kuersten, K. Lea, and T. Blumenthal, 1993 Operons in *C. elegans*:

1205   polycistronic mRNA precursors are processed by trans-splicing of SL2 to downstream

1206   coding regions. Cell 73: 521–532.

1207 Spike, C. A., D. Coetzee, C. Eichten, X. Wang, D. Hansen *et al.*, 2014a The TRIM-NHL protein

1208   LIN-41 and the OMA RNA-binding proteins antagonistically control the prophase-to-

1209   metaphase transition and growth of *Caenorhabditis elegans* oocytes. Genetics 198: 1535–

1210   1558.

1211 Spike, C. A., D. Coetzee, Y. Nishi, T. Guven-Ozkan, M. Oldenbroek *et al.*, 2014b Translational

1212   control of the oogenic program by components of OMA ribonucleoprotein particles in

1213   *Caenorhabditis elegans*. Genetics 198: 1513–1533.

1214 Spike, C. A., G. Huelgas-Morales, T. Tsukamoto, and D. Greenstein, 2018 Multiple mechanisms

1215   inactivate the LIN-41 RNA-binding protein to ensure a robust oocyte-to-embryo

1216   transition in *Caenorhabditis elegans*. Genetics 210: 1011–1037.

1217 Stitzel, M. L., J. Pellettieri, and G. Seydoux, 2006 The *C. elegans* DYRK kinase MBK-2 marks

1218   oocyte proteins for degradation in response to meiotic maturation. Curr Biol 16: 56–62.

1219 Teixeira, F. K., and R. Lehmann, 2019 Translational control during developmental transitions.

1220   Cold Spring Harb Perspect Biol 11: a032987.

1221 The *C. elegans* Deletion Mutant Consortium, 2012 Large-scale screening for targeted knockouts

1222   in the *Caenorhabditis elegans* genome. G3 (Bethesda) 2: 1415–1425.

1223   Timmons, L., and A. Fire, 1998 Specific interference by ingested dsRNA. Nature 395: 854.

1224   Tocchini, C., J. J. Keusch, S. B. Miller, S. Finger, H. Gut *et al.*, 2014 The TRIM-NHL protein

1225   LIN-41 controls the onset of developmental plasticity in *Caenorhabditis elegans*. PLoS

1226   Genet 10: e1004533.

1227   Torres-Fernández, L. A., J. Emich, Y. Port, S. Mitschka, M. Wöste *et al.*, 2021a TRIM71

1228   deficiency causes germ cell loss during mouse embryogenesis and is associated with

1229   human male infertility. Front Cell Dev Biol 9: 658966.

1230   Torres-Fernández, L. A., S. Mitschka, T. Ulas, S. Weise, K. Dahm *et al.*, 2021b The stem cell-

1231   specific protein TRIM71 inhibits maturation and activity of the pro-differentiation

1232   miRNA *let-7* via two independent molecular mechanisms. RNA 27: 805–828.

1233   Tsien, R. Y., 1998 The green fluorescent protein. Annu Rev Biochem 67: 509–544.

1234   Tsukamoto, T., M. D. Gearhart, C. A. Spike, G. Huelgas-Morales, M. Mews *et al.*, 2017 LIN-41

1235   and OMA ribonucleoprotein complexes mediate a translational repression-to-activation

1236   switch controlling oocyte meiotic maturation and the oocyte-to-embryo transition in

1237   *Caenorhabditis elegans*. Genetics 206: 2007–2039.

1238   van der Voet, M., M. A. Lorson, D. G. Srinivasan, K. L. Bennett, and S. van den Heuvel, 2009

1239   *C. elegans* mitotic cyclins have distinct as well as overlapping functions in chromosome

1240   segregation. Cell Cycle 8: 4091–4102.

1241   Wang, R., Z. Kaul, C. Ambardekar, T. G. Yamamoto, K. Kavdia *et al.*, 2013 HECT-E3 ligase

1242   ETC-1 regulates securin and cyclin B1 cytoplasmic abundance to promote timely

1243   anaphase during meiosis in *C. elegans*. Development 140: 2149–2159.

1244   Ward, S., Y. Argon, and G. A. Nelson, 1981 Sperm morphogenesis in wild-type and fertilization-

1245   defective mutants of *Caenorhabditis elegans*. J Cell Biol 91: 26–44.

1246   Welcker, M., and B. E. Clurman, 2008 FBW7 ubiquitin ligase: a tumour suppressor at the

1247   crossroads of cell division, growth and differentiation. Nat Rev Cancer 8: 83–93.

1248   Welcker, M., A. Orian, J. E. Grim, J. A. Grim, R. N. Eisenman *et al.*, 2004 A nucleolar isoform

1249   of the Fbw7 ubiquitin ligase regulates c-Myc and cell size. Curr Biol 14: 1852–1857.

1250   Worringer, K. A., T. A. Rand, Y. Hayashi, S. Sami, K. Takahashi *et al.*, 2014 The *let-7*/LIN-41

1251   pathway regulates reprogramming to human induced pluripotent stem cells by controlling

1252   expression of prodifferentiation genes. Cell Stem Cell 14: 40–52.

1253   Yoon, S., I. Kawasaki, and Y. H. Shim, 2017 The B-type cyclin CYB-1 maintains the proper

1254   position and number of centrosomes during spermatogenesis in. J Cell Sci 130: 2722–

1255   2735.

1256   You, J., and C. M. Pickart, 2001 A HECT domain E3 enzyme assembles novel polyubiquitin

1257   chains. J Biol Chem 276: 19871–19878.

1258   You, J., M. Wang, T. Aoki, T. A. Tamura, and C. M. Pickart, 2003 Proteolytic targeting of

1259   transcriptional regulator TIP120B by a HECT domain E3 ligase. J Biol Chem 278:

1260   23369–23375.

1261   Zavortink, M., L. N. Rutt, S. Dzitoyeva, J. C. Henriksen, C. Barrington *et al.*, 2020 The E2

1262   Marie Kondo and the CTLH E3 ligase clear deposited RNA binding proteins during the

1263   maternal-to-zygotic transition. Elife 9: e53889.

1264   Zevian, S. C., and J. L. Yanowitz, 2014 Methodological considerations for heat shock of the

1265   nematode *Caenorhabditis elegans*. Methods 68: 450–457.

1266

FIGURE LEGENDS

1267

1268   Figure 1. SEL-10 is expressed in oocytes and embryos and promotes the degradation of

1269   mSCARLET::LIN-41 during the OET. mSCARLET::LIN-41 (A, B, D, and F), GFP::SEL-10 (C)

1270   and SEL-10::GFP (E) fluorescence in *C. elegans* germlines (solid outlines) and early embryos

1271   (dashed outlines). mSCARLET::LIN-41 is rapidly degraded after oogenesis in the wild type (A)

1272   and *sel-10(tn1875[gfp::3xflag::sel-10])* (D) hermaphrodites but persists in early embryos in the

1273   *sel-10(ok1632)* deletion (B) and *sel-10(tn1817[sel-10::gfp::3xflag])* (F) hermaphrodites.

1274   Embryos with an increased amount of mSCARLET::LIN-41 relative to *sel-10(+)* embryos are

1275   outlined in magenta (B and F). Landmark structures such as the distal mitotic region of the

1276   germline (arrow in A), the proximal-most oocytes (arrowheads in A) and the spermatheca (sp),

1277   are indicated for reference. Scale bars, 100 μm.

1278

1279   Figure 2. SEL-10 degrades oocyte-expressed DENDRA::LIN-41. Red and green channel

1280   fluorescence (A–C and F–H) in DENDRA::LIN-41-expressing *sel-10(ok1632)* (A–E) and *sel-*

1281   *10(+)* (F–J) hermaphrodites. The positions of oocytes (solid outlines), embryos (dashed outlines)

1282   and spermathecae (sp) are indicated for reference. Images were collected either before

1283   photoactivation (A and F), immediately after photoactivation of the −1 oocyte (arrowheads, B

1284   and G) or after a 100-min recovery period (C–E and H–J). Embryos with above-background

1285   levels of red channel fluorescence are outlined in magenta; the embryo that most likely

1286   developed from the photoactivated −1 oocyte is indicated with an arrowhead (C and H).

1287   Magnified red channel fluorescence (D and I) and DIC images (E and J) of this embryo are

1288   shown. Scale bars, 50 μm (A–C and F–H) and 20 μm (D, E, I, and J).

60

1289

1290   Figure 3. PUF-11::GFP and PUF-3::GFP are degraded during the OET. (A–F) PUF-11::GFP (A),

1291   PUF-3::GFP (D and G) and mSCARLET::LIN-41 (B and E) fluorescence in *C. elegans*

1292   germlines (solid outlines) and early embryos (dashed outlines). The arrow in (A and D) indicates

1293   the distal mitotic region of each germline. Merged images of (A and B) and (D and E) are shown

1294   in (C) and (F), respectively. (G–J) Images of *itIs37[pie-1p::mcherry::histoneH2B::pie-1 3'UTR,*

1295   *unc-119(+)] puf-3(tn1820[puf-3::gfp::3xflag])* oocytes and embryos reveal that PUF-3::GFP (G)

1296   is strongly reduced in a meiosis I stage embryo (MI) relative to the −1 oocyte. Chromosomes are

1297   marked with mCHERRY:HISTONE (H), and the oocyte-derived chromosomes in this MI

1298   embryo appear to be aligning on the metaphase plate. PUF-3::GFP is at background levels in the

1299   adjacent post-meiotic 1-cell embryo (pn); this embryo has two polar bodies and maternal and

1300   paternal pronuclei at opposite ends of the embryo. Merged and DIC images of the same oocytes

1301   and embryos are shown in (I) and (J), respectively. The fluorescent images in this series (G–I)

1302   are 3D projections of a Z-stack. The DIC image (J) shows a single focal plane. Embryos with

1303   slightly higher levels of GFP and mSCARLET relative to older embryos are outlined in green

1304   and magenta, respectively (D, E, and G–J). Scale bars, 100 μm (A–F) and 50 μm (G–J). (K)

1305   PUF-3::GFP levels decrease after meiotic resumption. Mean GFP fluorescence was measured in

1306   images of *itIs37[pie-1p::mcherry::histoneH2B::pie-1 3'UTR] puf-3(tn1820)* oocytes and

1307   embryos and background-corrected. Fluorescence intensity is expressed relative to the amount of

1308   GFP fluorescence in the oldest oocyte with an intact nucleus; this is the −2 oocyte if the −1

1309   oocyte has initiated nuclear envelope breakdown (NEBD) or is starting to move into the

1310   spermatheca (early ovulation stage). Embryonic meiotic stage (e.g., metaphase I, telophase I and

1311   metaphase II) was classified based on the arrangement and organization of maternal

1312   chromosomes.

1313

1314   Figure 4. The elimination of PUF-3::GFP and PUF-11::GFP requires active CDK-1 but does not

1315   require SEL-10. PUF-3::GFP (A–D) and PUF-11::GFP (E–H) fluorescence in *C. elegans*

1316   germlines (solid outlines) and early embryos (dashed outlines) in *cdk-1(RNAi)* (A and E), *wee-*

1317   *1.3(RNAi)* (B and F), *lon-3(e2175)* (C and G) and *lon-3(e2175) sel-10(ar41)* (D and H)

1318   hermaphrodites. For each GFP fusion protein, the images of the *lon-3(e2175)* and *lon-3(e2175)*

1319   *sel-10(ar41)* animals were collected using the same settings (e.g., C and D). Embryos that appear

1320   GFP-positive are outlined in green. Arrowheads indicate the most proximal oocyte in each *wee-*

1321   *1.3(RNAi)* gonad that is strongly GFP-positive. The position of the spermatheca (sp) is indicated

1322   for reference. (I) This graph illustrates the relative position of the most proximal mSCARLET or

1323   GFP-positive oocyte in 12 different *lin-41(tn1892[mScarlet::3xflag:lin-41]); puf-11(tn1824[puf-*

1324   *11:gfp::3xflag]); wee-1.3(RNAi)* animals. *wee-1.3(RNAi)* animals with well-formed and

1325   organized oocytes were scored. Oocyte position was measured relative to other oocytes and the

1326   spermatheca (position 0). Each animal is represented by a different symbol (e.g., filled diamond

1327   or open circle). The color of the symbol represents the fusion protein that was scored:

1328   mSCARLET::LIN-41 in magenta and PUF-3::GFP in green. The vertical bar indicates the

1329   median. Scale bars, 50 μm (A–H).

1330

1331   Figure 5. *etc-1(gk5182)* perturbs the degradation of GFP-fusion proteins during the OET. PUF-

1332   3::GFP (A and B), PUF-11::GFP (C and D), CYB-1::GFP (E and F), mSCARLET::LIN-41 (G

1333 and H), IFY-1::GFP (I and J) and GFP$_F$::LIN-41 (K and L) fluorescence in young *etc-1(+)* (A, C,

1334 E, G, I, and K) and *etc-1(gk5182)* (B, D, F, H, J, and L) embryos. In each image, the position of

1335 the spermatheca (sp) is indicated for reference. Young embryos in the uterus are indicated with

1336 dashed outlines that highlight individual embryos (A–H, K, and L) or a bracket that indicates a

1337 region containing multiple post-meiotic embryos (I and J). GFP-positive embryos are indicated

1338 in green (A–F and I–L) while mSCARLET-positive embryos are indicated in magenta (G and

1339 H). For each fusion protein, these embryos contain detectably more fluorescence than the *etc-*

1340 *1(+)* embryos indicated in white. CYB-1::GFP re-accumulates to relatively high levels in older

1341 *etc-1(+)* embryos (E, arrowhead; this embryo is no longer in the uterus) and therefore has a

1342 distinctly different expression pattern than the other OET-degraded fusion proteins. Scale bars,

1343 50 µm.

1344

1345 Figure 6. ETC-1 is expressed in the *C. elegans* germline. (A) *etc-1* alleles and the exon-intron

1346 structure of *etc-1*, the downstream gene in operon CEOP2380. Exons are shown as open boxes;

1347 the region of exon 1 colored in pink would encode 20 additional amino acids if translation is

1348 initiated at ATG #1, the start codon immediately adjacent to the annotated SL1/SL2 trans-splice

1349 site (orange), instead of ATG #2. Other colors indicate the 3' UTR of the upstream gene eIF-2B

1350 (gray) and the regions that encode the conserved IQ (purple) and HECT (yellow) domains of

1351 ETC-1. (B) The N-terminus of ETC-1 aligned with the N-terminus of the human ortholog

1352 UBE3C; the amino acids predicted to be added to ETC-1 are in pink. This is the N-terminal

1353 portion of a full-length protein alignment generated by EMBOSS Needle with default alignment

1354 parameters. ETC-1 and UBE3C were 26% identical or 46% similar overall with 16% of the

1355 alignment gapped. (C and D) GFP::ETC-1 fluorescence in *C. elegans* germlines (solid outlines)

1356   and early embryos (dashed outlines). GFP is N-terminal to either the first (C, *etc-*

1357   *1(tn1919[gfp::3xflag::etc-1 #1])*) or second (D, *etc-1(tn1920[gfp::3xflag::etc-1#2])*) methionine

1358   of ETC-1. Scale bars, 100 μm. (E) A western blot of GFP::ETC-1 (~150 kDa, see main text) and

1359   PUF-3::GFP-expressing strains with an anti-FLAG antibody that recognizes both fusion proteins.

1360   GFP::FLAG fragments derived from PUF-3::GFP strongly accumulate in *etc-1(gk5182)* and *etc-*

1361   *1(tn1920[gfp::3xflag::etc-1#2])* hermaphrodites.

1362

1363   Figure 7. GFP-tagged fusion proteins are partially proteolyzed in *etc-1(gk5182)* animals. (A–E)

1364   Western blots with a FLAG-specific primary antibody. Three FLAG tags are located at the

1365   extreme C-terminus of PUF-3::GFP, PUF-11::GFP, CYB-1::GFP and IFY-1::GFP and in-

1366   between LIN-41 and each fluorescent protein (mSCARLET, DENDRA, or GFP). The predicted

1367   molecular mass of each full-length fusion protein (vertical line) is ~89 kDa for each PUF::GFP

1368   fusion protein (A and B), 73 kDa for CYB-1::GFP (A and B), 154–156 kDa for each LIN-41

1369   fusion protein (C and E), and 61 kDa for IFY-1::GFP (D). The same set of molecular weight

1370   markers (horizontal lines) were used in (A) and (B). A partially proteolyzed GFP::FLAG-

1371   containing fragment >32 kDa (arrow) accumulates in the *etc-1(gk5182)* animals that express a

1372   GFP fusion protein (A, B, D, and E). The protein lysates were made from adult hermaphrodites

1373   (A, C, D, and E), adult females (B) or adult males (B), as indicated.

1374

LEGENDS TO SUPPLEMENTAL FIGURES

1375

1376   Figure S1. Alleles used in this study. (A) The exon-intron structures and allele names of the *sel-*

1377   *10* alleles used in this study. Exons are shown as open boxes. Colored regions of the *sel-10* exons

1378   encode the conserved F box (orange) and 7 WD repeat (gray) domains found in SEL-10. The

1379   GFP and FLAG-encoding regions added to the GFP-tagged alleles are colored in green and cyan,

1380   respectively. (B) The exon-intron structures and allele names of the *lin-41* alleles used in this

1381   study. Colored regions of the *lin-41* exons encode the conserved RING (yellow), B-box (orange),

1382   BBC (blue), Ig/filamin (purple) and NHL repeats (red) domains found in LIN-41. Fusion protein

1383   tags include GFP (green), S tag (gray), mSCARLET-I (brick red), FLAG tag (cyan) and

1384   DENDRA (green to red color gradient). (C) The exon-intron structures and allele names of *puf-*

1385   *3::gfp::3xflag*, *puf-11::gfp::3xflag*, *cyb-1::gfp::3xflag* and *rnp-8::gfp::3xflag*. The Pumilio-like

1386   repeats of PUF-3 and PUF-11 are in yellow. The Cyclin-N and Cyclin-C motifs of CYB-1 are in

1387   blue and orange, respectively. The RNA recognition motif (RRM) present in RNP-8 is in purple.

1388   As in prior panels, the GFP and FLAG protein tags are in green and cyan, respectively.

1389

1390   Figure S2. GLD-1 is degraded normally in *sel-10(tn1875[gfp::3xflag::sel-10])* animals.

1391   Dissected wild-type (A and C), *sel-10(tn1875[gfp::3xflag::sel-10])* (B) and *sel-10(tn1816[sel-*

1392   *10::gfp::3xflag])* (D) gonads (solid outlines) that have been fixed and stained with an anti-GLD-

1393   1 antibody. Each gonad is oriented so that the distal mitotic region is on the left and the proximal

1394   oocyte-containing region is on the right. Two different wild-type gonads are shown because

1395   slightly different staining and imaging conditions were used for each experiment; wild-type

1396   image A pairs with *sel-10(tn1875[gfp::3xflag::sel-10])* (A-B) and wild-type image C pairs with

1397   *sel-10(tn1816[sel-10::gfp::3xflag])* (C and D). Scale bars, 50 μm.

1398

1399   Figure S3. The elimination of PUF-3/11::GFP proteins during the OET. (A–C) GFP expression

1400   in *puf-11(tn1824[puf-11::gfp::3xflag])* (A), *puf-3(tn1820[puf-3::gfp::3xflag])* (B) and *puf-*

1401   *11(tn1824); puf-3(tn1820)* (C) animals. GFP-positive embryos are outlined in green. All images

1402   were collected using the same settings. Scale bars, 100 μm.

1403

1404   Figure S4. GFP-expressing alleles of *etc-1*. (A) The exon-intron structures and allele names of

1405   the *gfp::3xflag::etc-1* alleles used in this study. Colors and labels are as described for Figure 6,

1406   with the addition of exons (open boxes) that encode the GFP (green) and FLAG (cyan) tags. (C

1407   and D) GFP fluorescence in *etc-1(tn1919[gfp::3xflag::etc-1#1])* (C) and *etc-*

1408   *1(tn1920[gfp::3xflag::etc-1#2])* (D) hermaphrodites. These are larger versions of the images

1409   shown in Figure 7 that include the region of somatic GFP expression in the head (arrow) that is

1410   significantly brighter in *etc-1(tn1920)* hermaphrodites. GFP expression in the nucleus of an

1411   intestinal cell is also evident in the focal plane of the *etc-1(tn1919)* image (arrowhead).

1412   Additional somatic cells also express GFP::ETC-1, but most of these cells were not identified.

1413   Scale bars, 100 μm.

1414

1415   Figure S5. Additional western blots related to Figure 7. (A) A western blot that repeats the

1416   experiment shown in Figure 7A and includes wild type and *etc-1(gk5182)* lanes with no

1417   GFP::FLAG fusion protein. (B) PUF::GFP, PUF-11::GFP, and CYB-1:: GFP fusion proteins

1418   (lines) and *etc-1(gk5182)*-specific GFP::FLAG fragments (arrows) are detected by an affinity

1419   purified antibody that recognizes GFP. (C and D) Western blots with the anti-FLAG antibody on

1420   GFP fusion protein-expressing hermaphrodites (C), mated *fog-2(oz40)* females (C), unmated *fog-*

1421   *2(oz40)* females (D) and *fog-2(oz40)* males (D) with the indicated *etc-1* genotypes. For unknown

1422   reasons, the RNP-8::GFP fusion protein detected in (C) appears to be slightly larger than

1423   predicted. The predicted size of the large RNP-8a isoform (see http://www.wormbase.org,

1424   release WS278) fused to the GFP::3xFLAG tag is 97 kDa. The blots shown in (D) and Figure 7B

1425   are the same; Figure 7B shows a shorter exposure of the portion of the blot with the female

1426   lysates and a longer exposure of the blot with the male CYB-1::GFP lysates. (E) A longer

1427   exposure of the western blot shown in Figure 7C that also includes otherwise wild-type, *etc-*

1428   *1(gk5182)* and *sel-10(lf)* animals that express DENDRA::LIN-41. (F) A longer exposure of the

1429   western blot shown in Figure 7E. *etc-1(+)* animals that express GFP$_F$::LIN-41 appear to

1430   accumulate a lesser amount of the GFP::FLAG fragment seen in *etc-1(gk5182)* animals. *etc-*

1431   *1(gk5182)*-specific fragments containing GFP::FLAG are indicated by arrows.

1432

1433   Figure S6. CYB-1::GFP expression in males. (A–F) CYB-1::GFP expression in *etc-1(+)* males

1434   (A) and *etc-1(gk5182)* males (C and F). CYB-1::GFP disappears abruptly in *cyb-1(tn1806[cyb-*

1435   *1::gfp::3xflag]); fog-2(oz40)* males (A and B) near the end of spermatogenesis (red boxes). At

1436   the same stage of spermatogenesis, *etc-1(gk5182)*; *cyb-1(tn1806[cyb-1::gfp::3xflag]); fog-*

1437   *2(oz40)* males (C–F) have higher levels of GFP fluorescence (C) and GFP-positive residual

1438   bodies (e.g., arrows in E and F). Scale bars, 50 μm (A–D) and 10 μm (E and F).
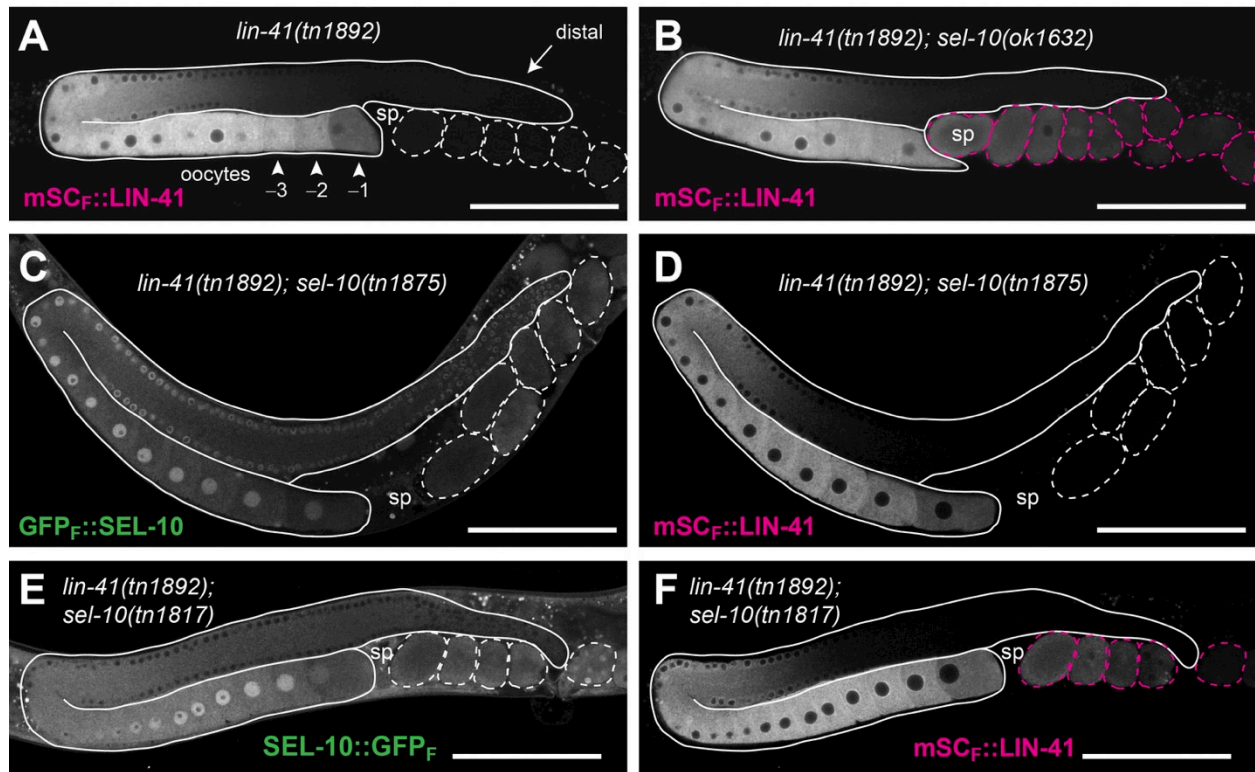
67

1439

1440   Figure S7. Additional images of GFP-tagged fusion proteins. (A and B) GFP is expressed at

1441   similar levels in the germlines (solid outlines) and early embryos (dashed outlines) of *rnp-*

1442   *8(tn1860[rpn-8::gfp::3xflag])* (A) and *etc-1(gk5182); rnp-8(tn1860[rpn-8::gfp::3xflag])* (B)

1443   hermaphrodites. (C and D) GFP fluorescence from *lin-41(tn1541[gfp::s::lin-41])* is distinctly

1444   brighter in the early embryos (dashed outlines) of *etc-1(gk5182)* hermaphrodites (D) relative to

1445   *etc-1(+)* hermaphrodites (C). (E–H) The GFP$_S$-tagged allele *lin-41(tn1541[gfp::s::lin-41])* (E)

1446   and GFP$_F$-tagged allele *lin-41(tn2054[gfp::3xflag::lin-41])* (G) have different levels of GFP

1447   expression. The average GFP fluorescence intensity in the cytoplasm of the −1 and −2 oocytes of

1448   *lin-41(tn2054)* and *lin-41(tn1541)* Day 1 adult hermaphrodites was measured (n=7 images for

1449   each allele, collected as shown). At each oocyte position (−1 or −2), the average background-

1450   corrected level of fluorescence was 2.4-fold higher in *lin-41(tn2054)* oocytes relative to *lin-*

1451   *41(tn1541)* oocytes ($P < 1 \times 10^{-6}$). Many *lin-41(tn2054[gfp::3xflag::lin-41])* Day 1 adult

1452   hermaphrodites also accumulate older embryos in their uterus (H) and appear to be sluggish.

1453   These phenotypes are shared by the independently-generated *lin-41(tn2055[gfp::3xflag::lin-41]*

1454   allele. At 20 °C, 43% and 62% of DG5263 *lin-41(tn2055)* Day 1 and Day 2 adults (n=29),

1455   respectively, had an egg laying (Egl) defect associated with premature mortality (dead on Day 2,

1456   3, or 4 of adulthood) and a reduced number of progeny (52 ± 21 larvae, n=18 Egl adults; 256 ±

1457   61 larvae, n=11 non-Egl adults). These somatic defects are not typically seen in *lin-*

1458   *41(tn1541[gfp::s::lin-41])* animals at the same stage of adulthood (F), and the average brood size

1459   of *lin-41(tn1541)* animals is greater than 300 (Spike *et al.* 2014a, 2018). (I–N) GFP fluorescence

1460   (I, K, and M) and DIC (J, L, and N) images of 2-cell *lin-41(tn2055[gfp::3xflag::lin-41])*

1461   embryos produced by otherwise wild-type (I and J), *etc-1(gk5182)* (K and L) and *sel-10(ok1632)*

1462   (M and N) parents. GFP is diffusely cytoplasmic in each embryo and is distinctly brighter in the

1463   *etc-1(gk5182)* and *sel-10(ok1632)* embryos relative to the wild-type embryo. Nuclear GFP

1464   (arrowheads) is evident in wild-type (I) and *etc-1(gk5182)* (K) embryos. In contrast, some GFP

1465   in the posterior blastomere of the *sel-10(ok1632)* embryo (M) appears to associate with P

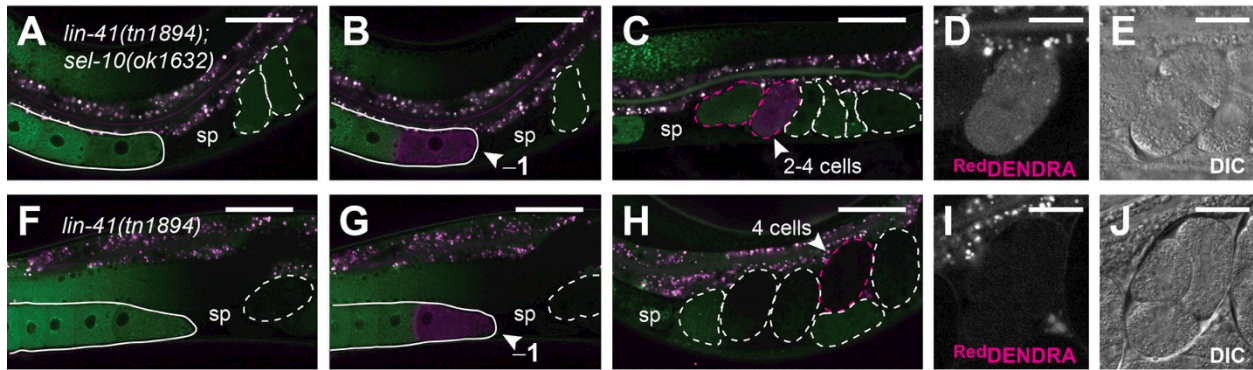1466   granules (arrow). Scale bars, 50 μm (A–H) and 10 μm (I–N).

1467

Figure 1

1468

1469

Figure 2

1470
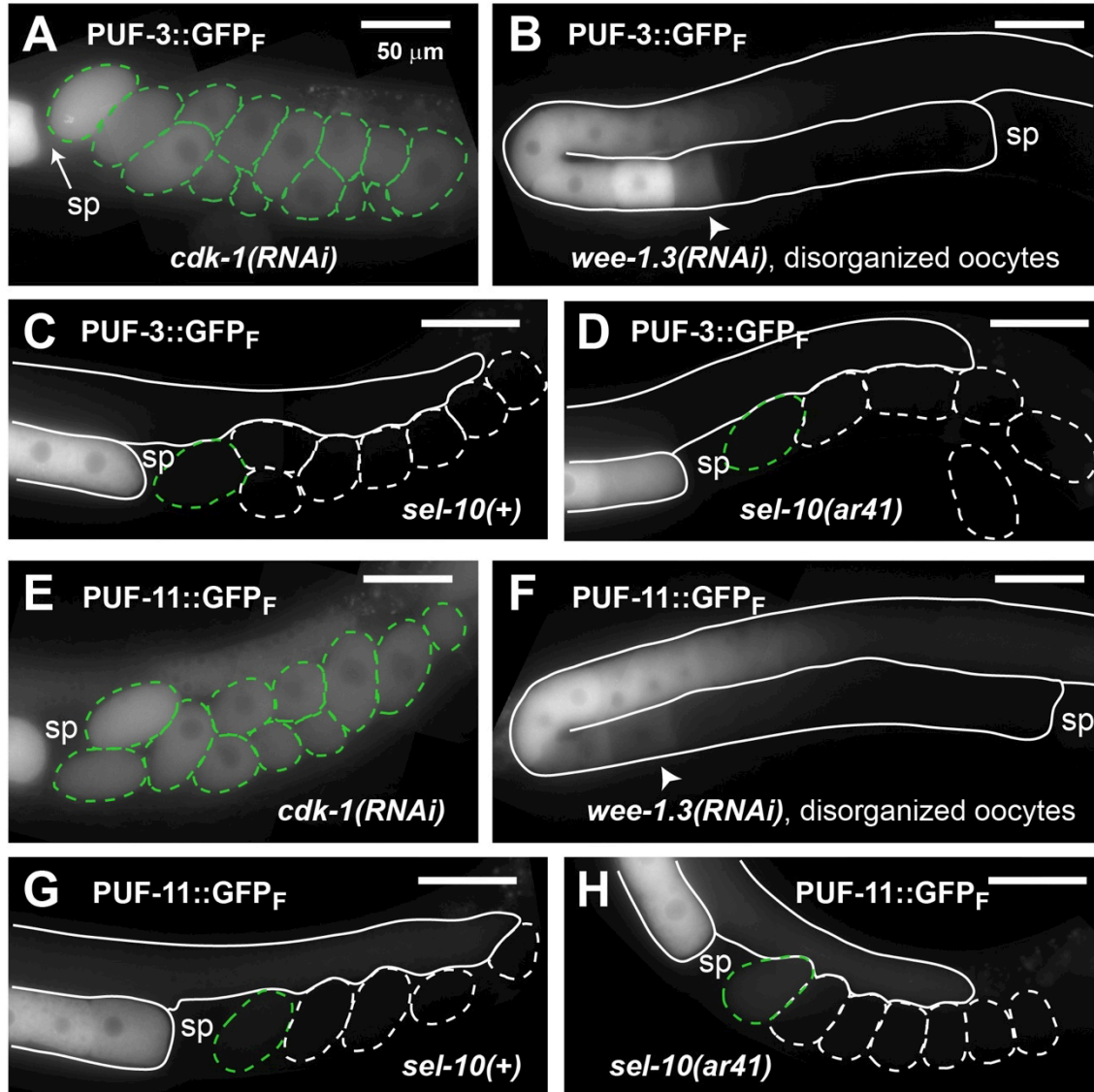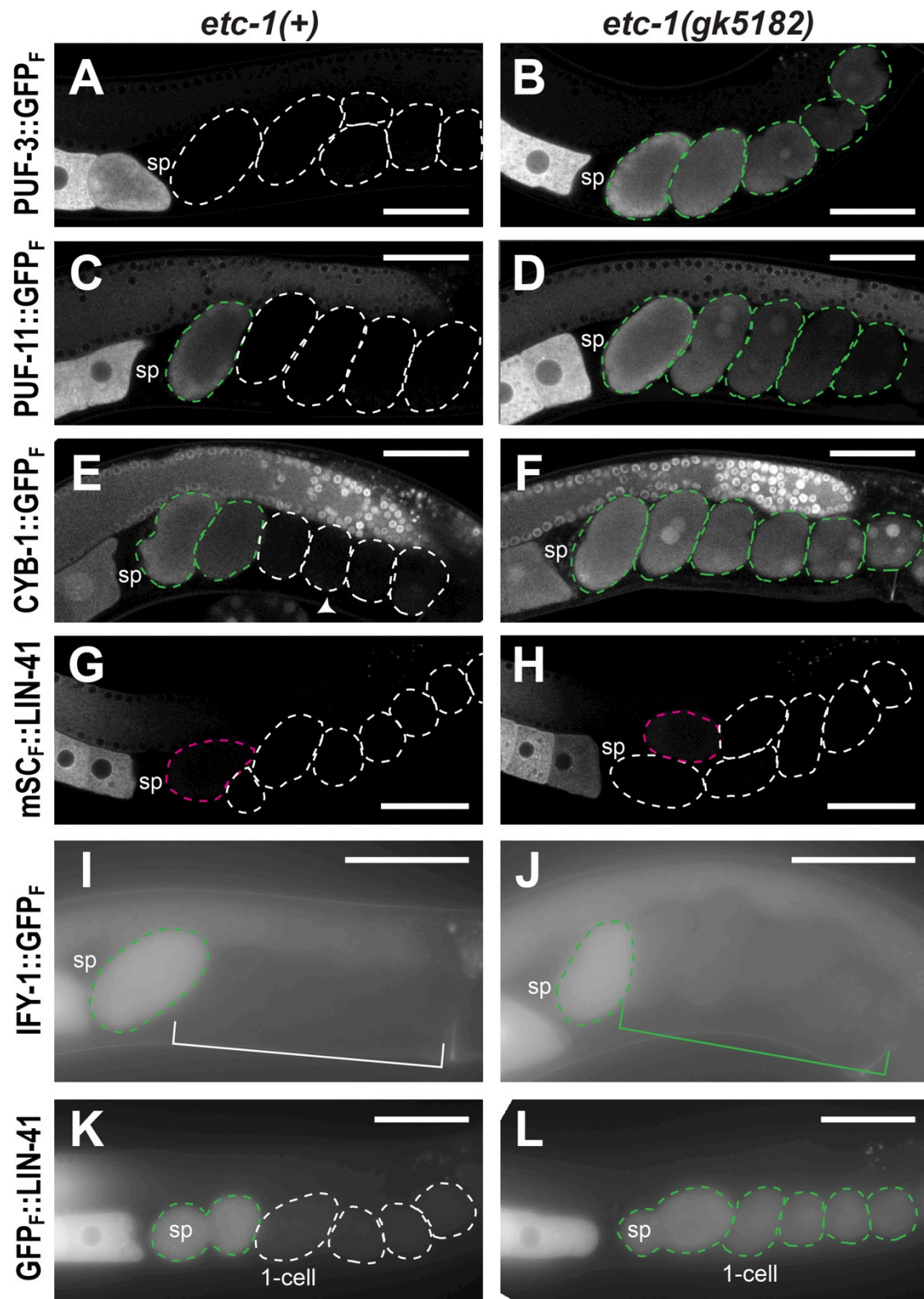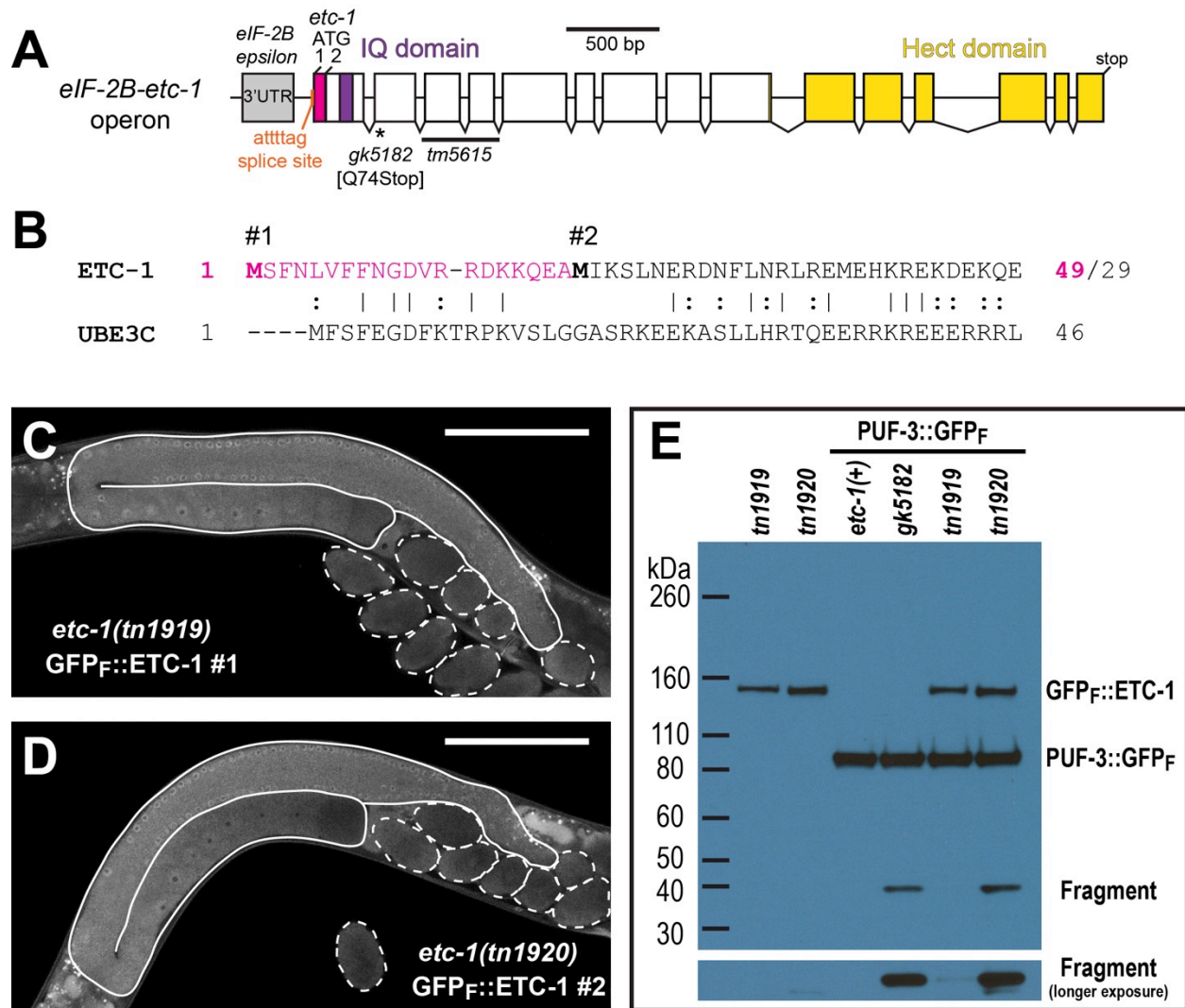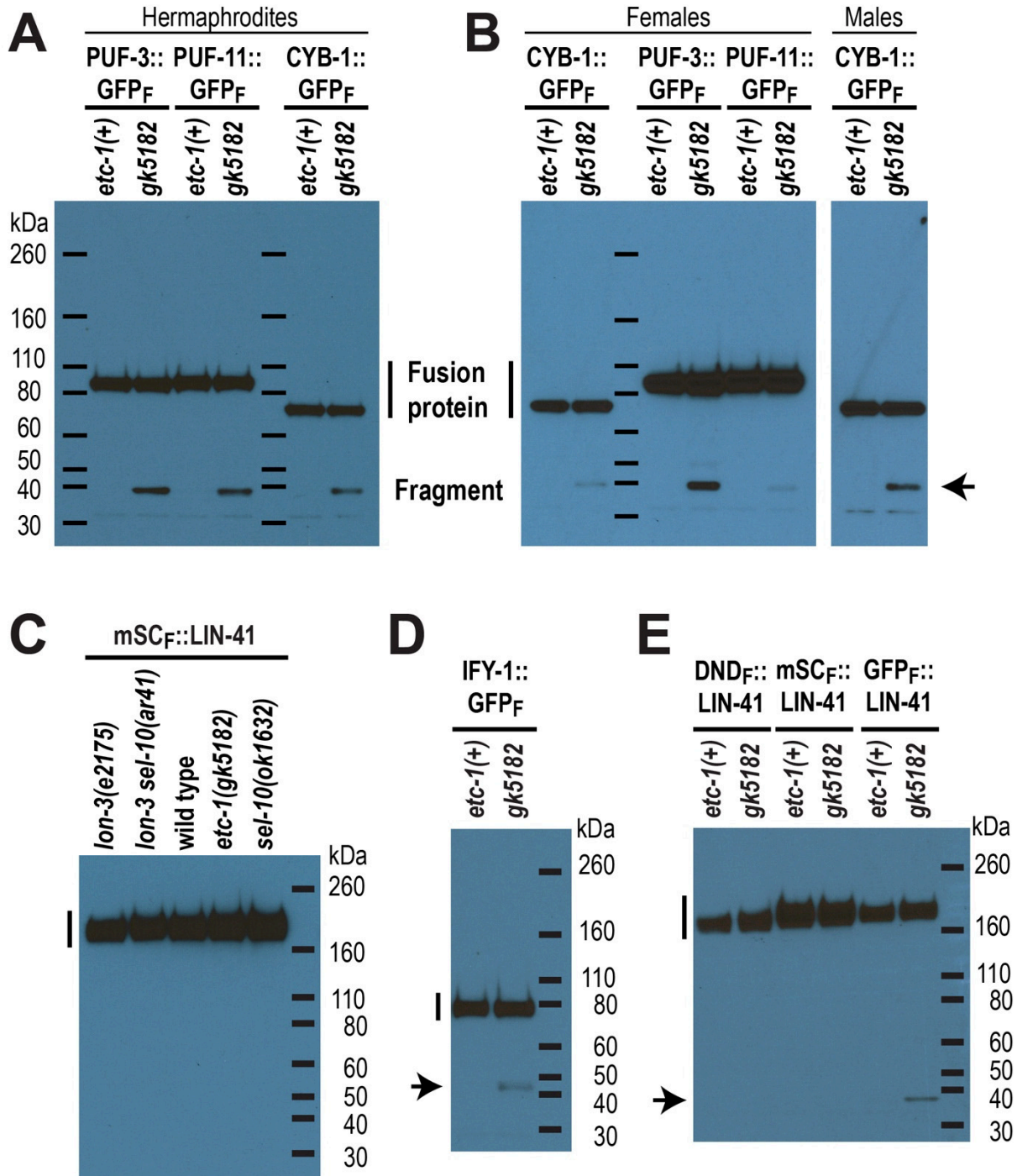
1471

Figure 3

1472

Figure 4

1473

Figure 5

1474

Figure 6

B

```
         #1                              #2
ETC-1  1  MSFNLVFFNGDVR-RDKKQEAMIKSLNERDNFLNRLREMEHKREKDEKQE  49/29
          :  | || : | |        |: : |:| :|   |||:: ::
UBE3C  1  ----MFSFEGDFKTRPKVSLGGASRKEEKASLLHRTQEERRKREEERRRL  46
```

1475

1476

75

Figure 7

1477

1478